의학박사 학위논문

Metabolomics study to explore pathophysiology and discover diagnostic biomarkers of idiopathic inflammatory myopathy

대사체학 기반 특발성 염증성 근육병증의 기전 탐색 및 진단 바이오마커 발굴

2023년 8월

서울대학교 대학원

의과학과 의과학전공

강 지 현

Ph.D. Dissertation of Medical Science

대사체학 기반 특발성 염증성 근육병증의 기전 탐색 및 진단 바이오마커 발굴

Metabolomics study to explore pathophysiology and discover diagnostic biomarkers of idiopathic inflammatory myopathy

August 2023

Seoul National University Graduate School
Department of Biomedical Sciences
Major in Biomedical Sciences

Jihyun Kang

대사체학 기반 특발성 염증성 근육병증의 기전 탐색 및 진단 바이오마커 발굴

지도교수 조 주 연

이 논문을 의학박사 학위논문으로 제출함

2023년 4월

서울대학교 대학원

의과학과 의과학전공

강 지 현

강지현의 의학박사 학위논문을 인준함

2023년 7월

위 원 장 _____ (인)

부위원장 _____ (인)

위 원 _____ (인)

위 원 _____ (인)

위 원 _____ (인)

Metabolomics study to explore pathophysiology and discover diagnostic biomarkers of idiopathic inflammatory myopathy

Joo-Youn Cho

Submitting a Ph.D. Dissertation of
Medical Science

April 2023

Seoul National University Graduate School
Department of Biomedical Sciences
Major in Biomedical Sciences

Jihyun Kang

Confirming the Ph.D. Dissertation written by
Jihyun Kang

July 2023

Chair	(Seal)
Vice Chair	(Seal)
Examiner	(Seal)
Examiner	(Seal)
Examiner	(Seal)

Abstract

Metabolomics study to explore pathophysiology and discover diagnostic biomarkers of idiopathic inflammatory myopathy

Jihyun Kang

Major in Biomedical Sciences

Department of Biomedical Sciences

Seoul National University Graduate School

INTRODUCTION: Idiopathic inflammatory myopathy (IIM) is a diverse set of autoimmune diseases with various clinical symptoms, responses to treatment, and prognoses. The diagnosis for IIM can be challenging without conducting muscle biopsy. In this study, a panel of metabolites were identified through a metabolomics approach in serum samples for IIM detection. The metabolomic signature of IIM was investigated using both human serum samples and tissue samples from a mouse model.

METHODS: Serum samples from 50 IIM patients, 30 ankylosing spondylitis (AS) patients, and 10 healthy volunteers as well as muscle

tissue samples from C-protein-induced myositis (CIM) which is a murine model of IIM were collected. All samples were subjected to a targeted liquid chromatography–mass spectrometry-based metabolomic approach, and part of human serum samples underwent an untargeted metabolomics approach. Three machine learning methods, namely logistic regression (LR), support vector machine (SVM), and random forest (RF), were applied to build prediction models for IIM patients. In addition, univariate and multivariate statistical analyses, as well as pathway enrichment analysis, were performed on serum and tissue samples to identify metabolic alterations.

RESULTS: ANOVA revealed 37 IIM-specific metabolites and a set of 7 predictive metabolites was calculated by backward stepwise selection. The discrimination model for IIM was evaluated within 5-fold cross-validation by using three machine learning algorithms. The model produced area under the receiver operating characteristic curve values of 0.955 (LR), 0.908 (RF), and 0.918 (SVM). Additionally, the analysis of subset of human serum samples revealed a significant increase in oxylipins in the IIM group. In mouse tissue samples, a total of 68 metabolites were significantly changed in CIM mice. The metabolic profiles of CIM mice showed a consistent pattern among all metabolites from various classes, except for taurine. Notably, the polyamine pathway and the beta-alanine pathway were identified as

the pivotal pathways implicated in the inflammatory response of muscle tissue in CIM mice.

CONCLUSION: A metabolomics-based approach was employed to identify potential biomarkers of IIM and uncover the relevant metabolic pathways involved in the underlying pathological processes of IIM.

* Part of this work has been published as original article in *Metabolites* (Kang J and Kim J, et al. Identification of Metabolic Signature Associated with Idiopathic Inflammatory Myopathy Reveals Polyamine Pathway Alteration in Muscle Tissue. Metabolites. 2022;12(10))

KEYWORDS: idiopathic inflammatory myopathy, metabolomics, C protein-induced myositis, biomarker, pathophysiology

STUDENT NUMBER: 2017-25272

Table of Contents

List of Figures

List of Tables

Introduction

Idiopathic inflammatory myopathy (IIM) is a group of rare autoimmune diseases characterized by immune-mediated myositis that leads to progressive proximal muscle weakness. It is often accompanied by various extramuscular manifestations, including skin rash, arthritis, and interstitial lung disease (1). Despite extensive research efforts, the exact etiology and underlying molecular mechanisms driving the pathogenesis of IIM remain incompletely understood (2). The complex interplay between genetic and environmental factors, as well as immune dysregulation, is considered to contribute to the complex of IIM (3). The incidence and prevalence of IIM remain unclear, but a systemic review reported an incidence ranged from 1.16 to 19 cases per million per year and a prevalence ranging from 2.4 to 33.8 per 100,000 inhabitants (4). Moreover, the incidence of IIM is gradually increasing, which may reflect the advances in diagnostic technologies.

In 1975, Bohan and Peter suggested the diagnostic criteria of IIM, especially polymyositis (PM) and dermatomyositis (DM), which are predominantly used despite certain limitations (5, 6). The recent discovery of myositis-specific auto-antibodies (MSAs) and myositis-associated auto-antibodies (MAAs), which are present in up to 60% of IIM patients, has majorly advanced the diagnosis of IIM (7). However,

a disadvantage of this technique is its limited availability, and approximately 40% of IIM patients do not exhibit these antibodies (8). Therefore, a muscle biopsy is necessary if the diagnosis cannot be confirmed based on clinical and laboratory findings. However, histopathologic findings are often insufficient for diagnosis because of the patchy distribution of inflammatory foci in muscle tissue or due to the use of medication prior to the pathologic diagnosis.

C protein-induced myositis (CIM) is a murine model of polymyositis (PM) that is induced by a single immunization with recombinant skeletal muscle C protein fragments in C57BL/6 mice. Infiltration of CD8+ T cells is the primary mechanism of muscle injury, and increased levels of interleukin (IL)-1, IL-6, and tumor necrosis factor (TNF)-α are crucial indicators of the development of CIM (9-11). Due to the challenges associated with collecting muscle tissues from humans, studying the inflammatory processes occurring in muscles has been difficult. Consequently, the CIM model tissue was used to investigate the pathology of PM for its comparable disease mechanism in this study.

Ankylosing spondylitis (AS) is one of chronic inflammatory diseases causing axial arthritis, resulting spinal structural damage (12). It mainly affects the sacroiliac joints that connect the base of the spine. AS is also an autoimmune disease characterized by inflammatory back pain and spinal stiffness (12). Muscle involvement has uncommonly been reported in AS patient (13). Therefore, the serum of AS patients

was evaluated as a disease control group to identify specific metabolite profiles when inflammation targets the muscle.

Previous studies reported genetic and environmental risk factors associated with IIM, including muscle weakness and damage to immune and non-immune mechanisms (14). The metabolome, which represents a set of metabolites, can be analyzed to discover biomarkers and describe interactions among genotype, diet, and environmental factors to elucidate the molecular mechanisms involved in IIM (15). Furthermore, tissue metabolomics allows informing the localized effects of environmental factors and complex interactions that occur at the direct site of pathogenesis (16). Metabolic alterations have been reported in IIM patients, describing metabolic dysregulation in serum and muscle tissues (17). Key metabolic pathways, including anaerobic metabolism, oxidative defects, and muscle catabolism, were evaluated through metabolomics (17). However, none of the previous studies analyzed serum biomarkers using metabolomics to classify IIM or aid in diagnosis. This study was conducted with the aim of identifying the metabolite panel as a potential biomarker for differentiating IIM from controls or disease controls and exploring the metabolic signature of IIM pathology by using tissue samples from mouse model and serum samples from IIM patients, AS patients, and healthy controls.

Methods

1. Study participants[A]

Patients were recruited from Seoul National University Hospital from March 2010 to February 2020. Patients with IIM who were 19 years or older and diagnosed according to probable or definite PM or DM based on the Bohan and Peter criteria were eligible for inclusion (5, 6). Patients with other rheumatic diseases were excluded. The reference group was composed of patients with AS, and the healthy control group included participants without any immune-mediated disease. AS is a chronic inflammatory autoimmune disease that mainly affects spine joints, causing severe, chronic pain, and IIM is a chronic inflammatory disease of unknown etiology that may affect the skin, muscles, and lungs. These two autoimmune diseases have different etiopathogeneses as well as clinical and genetic characteristics. In this study, the serum of AS patients was compared and analyzed as a disease control. The diagnosis of AS was based on the 1984 Modified New York Criteria for AS.

Serum samples of the participants were obtained once at the enrollment date. Information on demographics, including age, sex,

[A] Patient recruitment, sample collection, and laboratory assessment were conducted by Prof. Eun Young Lee.

and body mass index (BMI, kg/m^2), was collected from all participants. In addition, the following information was collected from IIM patients: clinical manifestations at IIM onset, including proximal muscle weakness, skin rash, dyspnea, dysphagia, Raynaud's phenomenon, and arthralgia; previous treatment history of glucocorticoids, intravenous immunoglobulin, or immunosuppressive agent use; laboratory results including white blood cell count, creatinine kinase, aldolase, myoglobin, lactate dehydrogenase, erythrocyte sedimentation rate, and C-reactive protein at the sampling date and positivity of antinuclear antibodies and anti-Jo-1 (anti-histidyl-transfer RNA synthetase antibody). The results of the diagnostic tests for myositis, including electromyography, muscle biopsy, chest computed tomography, and pulmonary function test, were also retrieved.

Written informed consent was obtained from all participants before their enrollment in the trial. This study was approved by the institutional review board of the Seoul National University Hospital (study identification number: g1103-151-357 and 1902-120-1013) and was conducted in accordance with the Declaration of Helsinki.

2. Induction of C protein-induced myositis

C57BL/6 mice were purchased from OrientBio (Sungnam, Korea). Female mice (age 8 to 10 weeks) were immunized intradermally with 200 μg C-protein fragments emulsified in complete Freund's adjuvant containing 100 μg heat-killed *Mycobacterium butyricum* (Difco, Franklin Lakes, NJ, USA) (9). The immunogens were injected at multiple sites over the back and into the foot pads, and 250 ng pertussis toxin (Sigma-Aldrich, St. Louis, MO, USA) diluted with 0.03% Triton X was injected intraperitoneally. A total of 26 mice were sacrificed on day 14 after immunization, and the sera and proximal muscles (hamstring and quadriceps) of both hind legs were harvested.

3. Histological Analysis[B]

Hematoxylin and eosin-stained 10-μm sections of the proximal muscles were examined histologically for the presence of mononuclear cell infiltration and necrosis of muscle fibers. The histologic severity of inflammation in each muscle block was graded as Grade 1, involvement of a single muscle fiber; Grade 2, a lesion involving 2–5 muscle fibers; Grade 3, a lesion involving 6–15 muscle fibers; Grade 4, a lesion involving 16–30 muscle fibers; Grade 5, a lesion involving 31–100 muscle fibers; and Grade 6, a lesion involving >100 muscle fibers. When multiple lesions with the same grade were found in a single muscle section, an additional 0.5 points was added to the grade. The histologic grading was based on a method that was modified from that of Sugihara et al. (9). All experiments were done under specific pathogen-free conditions. The animal experiment was approved by the Institutional Animal Care and Use Committee of Seoul National University Hospital [IACUC No. 15-0058-C1A1].

[B] Histological analysis has been performed by Jeong Yeon Kim and Prof. Eun Young Lee and previously reported by Jihyun Kang and Jeong Yeon Kim (Kang J and Kim J, et al. Identification of Metabolic Signature Associated with Idiopathic Inflammatory Myopathy Reveals Polyamine Pathway Alteration in Muscle Tissue. Metabolites. 2022;12(10)).

4. Mass spectrometry-based analyses

4.1. Mass spectrometry-based targeted metabolomics analysis

Serum and tissue metabolites were measured by using the Biocrates AbsoluteIDQ p180 platform (BIOCRATES Life Sciences AG, Innsbruck, Austria) (Figure 1). This high-throughput metabolome platform combines a flow-injection analysis and liquid chromatography method that enables the quantification of amino acids, acylcarnitines, sphingomyelins (SMs), lysophosphatidylcholines (lysoPCs), phosphatidylcholines (PCs), hexoses, and biogenic amines. These assays were analyzed using API 4000 QTRAP (AB Sciex, Framingham, MA, USA) equipped with an Agilent 1200 series high-performance liquid chromatography (HPLC) system (Agilent Technologies, Santa Clara, CA, USA) and an AB SCIEX 5500 QTrap mass spectrometer (AB Sciex, USA) equipped with a Waters ACQUITY ultra-performance liquid chromatography (UPLC) I-Class (Waters, Milford, MA, USA) with electrospray ionization. The concentration of each metabolite was measured in ng/mL. The calibration standards, internal standards, quality controls, and 10 μL of human and mouse samples were applied onto the 96-well extraction plate and dried under nitrogen gas. After derivatization, all metabolites were extracted for mass spectrometry analysis. Additionally, 17 bile acids were quantified using Biocrates

bile acid kit (BIOCRATES Life Sciences AG, Innsbruck, Austria) in part of human serum. The kit detects 20 bile acids and for further analysis, the following 16 specific human bile acids were selected: cholic acid (CA), chenodeoxycholic acid (CDCA), deoxycholic acid (DCA), lithocholic acid (LCA), ursodeoxycholic acid (UDCA), glycocholic acid (GCA), glycochenodeoxycholic acid (GCDCA), taurocholic acid (TCA), taurochenodeoxycholic acid (TCDCA), tauromuricholic acid (TMCA (a+b), glycodeoxycholic acid (GDCA), glycolithocholic acid (GLCA), taurodeoxycholic acid (TDCA), taurolithocholic acid (TLCA), glycoursodeoxycholic acid (GUDCA), glycoursodeoxycholic acid (TUDCA).

4.2. Mass spectrometry-based untargeted metabolomics analysis

The part of human serum samples also was analyzed using untargeted metabolomics platform (Figure 1). The 70 μL of plasma sample of human serum was mixed with 280 μL of pre-chilled 1:1 acetonitrile/methanol (v/v) and vortexed briefly. The mixture was centrifuged at 14,000 g for 10 mins. 4 μL of aliquot samples were injected and separated using a 2.1 mm × 100 mm ACQUITY 1.8 μm HSS T3 column. All samples were analyzed using a Q-Exactive Plus™ quadrupole-Orbitrap mass spectrometer (Thermo Fisher Scientific, United States) with an Ultimate 3000 UPLC system (Dionex, United

States) that was controlled with Thermo Xcalibur software (Thermo Fisher Scientific, United States). The mobile phase was composed of 0.1% formic acid (solvent A) and methanol containing 0.1% formic acid (solvent B) at a flow rate of 0.4 ml/min. The gradient started at 5% B, reached 95% B from 12 to 23 minutes, and was maintained at 5% B from 23 to 25 minutes. Pooled Quality control (QC) replicates were analyzed with samples for consistency and stability.

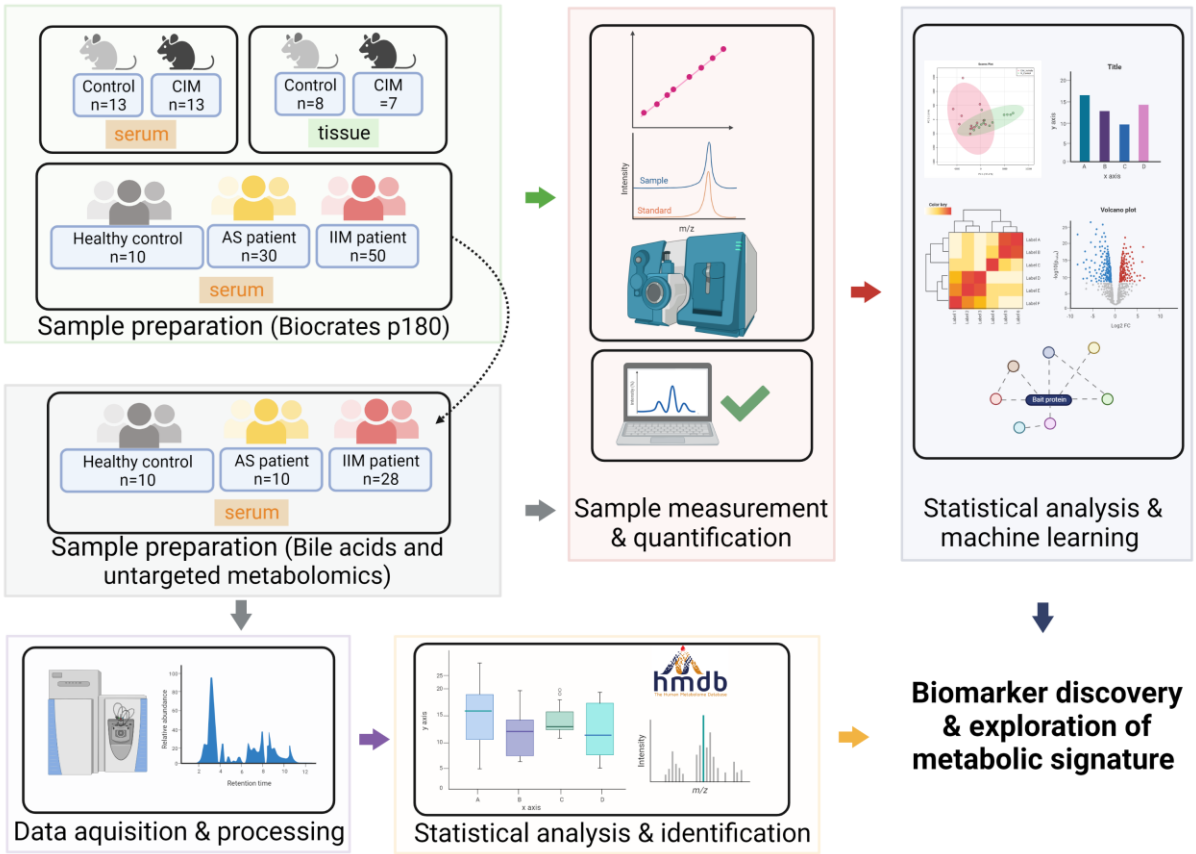

Figure 1. Study workflow of this study

5. Raw data processing and normalization

5.1. Targeted metabolomics raw data processing using MetIDQ

The raw data from LC -MS/MS mode was confirmed using Analyst software 1.6.3 (ABSciex, Framingham, MA, USA) and the quantitative generated data from FIA-MS/MS mode was generated using MetIDQ software (BIOCRATES Life Sciences AG, Innsbruck, Austria). Two batches, including all human and mouse samples, were normalized with standardized quality control to adjust the batch effect. After normalization, data were analyzed with MetaboAnalyst 5.0 (18). A missing value refers to an observed value that is below the limit of detection or the absence of a metabolite. Metabolites with 50% missing values were excluded, and the remaining missing values were imputed with 1/5 of the minimum positive value of each variable.

5.2. Untargeted metabolomics raw data processing

Raw data were imported into Progenesis QI software (version 2.3; Nonlinear Dynamics, Newcastle, UK). Peak alignment, peak picking, deconvolution, normalization, and statistical analysis were performed. using pooled QC replicates. Minimum peak width was set at 0.02 min.

Metabolic features with a coefficient of variation <30% were filtered to remove unstable metabolites.

6. Protein Extraction and Western Blot Analysis[C]

Skeletal muscles were extracted using a lysis buffer containing 20 mM Hepes-NaOH (pH 7.0), 0.15 M NaCl, 10% glycerol, 1% Nonidet P-40, 1 mM EDTA, 1 mM EGTA, 10 mM β-phosphoglycerate, 1 mM sodium vanadate, 5 mM NaF, 1 mM trichostatin A, and 20 mM nicotinamide, along with a mixture of protease inhibitor and phosphatase inhibitor (Sigma Aldrich, St. Louis, MO, USA). The lysates were centrifuged to remove debris, and the supernatants were used for immunoblot analysis. The final protein concentrations were determined using the Bradford protein assay (Bio-Rad, Hercules, CA, USA). The protein extracts were subjected to SDS-PAGE gel (8–15%), and NuPAGE Novex 4–12% Bis-Tris gel electrophoresis (Invitrogen) and electrophoresis were carried out using sodium dodecyl sulfate-10% polyacrylamide gels electrophoresis (SDS-PAGE). The separated proteins were transferred to a polyvinylidene difluoride membrane. The membrane was incubated overnight at 4 °C with primary antibodies (ODC-1 (Abcam), SMOX (Abcam), tubulin (cell signaling)) and then for 1 h at room temperature with horseradish peroxidase-conjugated secondary antibodies and enhanced chemiluminescence reagents (ELPIS

[C] Protein extraction and western blot analysis has been performed by Jeong Yeon Kim and Prof. Eun Young Lee and previously reported by Jihyun Kang and Jeong Yeon Kim (Kang J and Kim J, et al. Identification of Metabolic Signature Associated with Idiopathic Inflammatory Myopathy Reveals Polyamine Pathway Alteration in Muscle Tissue. Metabolites. 2022;12(10)).

Biotech, Daejeon, Korea). Films were scanned, and optical densities were quantified using ImageJ software.

7. Enzyme-linked immunosorbent assay[D]

Serum cytokines were determined by using interleukin 6 (IL-6), interleukin-1β (IL-1β), and Tumor necrosis factor alpha (TNF-α), enzyme-linked immunosorbent assay (ELISA) kits (R&D Systems, Minneapolis, MN, USA).

[D] ELISA has been performed by Jeong Yeon Kim and Prof. Eun Young Lee and previously reported by Jihyun Kang and Jeong Yeon Kim (Kang J and Kim J, et al. Identification of Metabolic Signature Associated with Idiopathic Inflammatory Myopathy Reveals Polyamine Pathway Alteration in Muscle Tissue. Metabolites. 2022;12(10)).

8. Statistical analysis

8.1. Normalized targeted metabolomics data

Multivariate, univariate, cluster and enrichment pathway analyses were performed in MetaboAnalyst 5.0 (18). Significant metabolites were selected with a false discovery rate (FDR) adjusted p-value less than 0.05 by using the Kruskal-Wallis one-way analysis of variance (ANOVA) followed by Dunn's post hoc test for human serum samples and by using the non-parametric t-test for mouse samples. All individual graph of significant metabolites was generated using GraphPad Prism software. Model and machine learning analyses were performed using R software (version 4.2.0). The number of significant metabolites was reduced by backward stepwise selection. A predictive model was established using logistic regression (LR), random forest (RF), and a support vector machine (SVM). The receiver operating characteristic (ROC) curve was used for the evaluation of model performance. Additionally, network analysis was processed with an FDR-adjusted p-value, fold change and fold change direction by using MetaMapp and was visualized using Cytoscape. The differential metabolites between CIM and control group were uploaded to the enrichment analysis in Metaboanalyst 5.0 by applying HMDB identifiers. Significant pathways were selected using p-value.

8.2. Untargeted metabolomics data

After raw data processing, further analysis was subjected to multivariate statistical analysis by EZinfo 2.0 software (Umetrics, Umea, Sweden). Principal component analysis (PCA) with pareto scaling algorithm was applied for detecting the dominant patterns and grouping. Additional statistical analysis for selecting significant metabolites (FDR adjusted p-value < 0.05) were performed in Progenesis QI.

Results

1. Clinical characteristics of the participants

From March 2010 to August 2019, a total of 50 patients with IIM, 30 patients with AS, and 10 healthy controls were enrolled in the study. The demographic characteristics of the study population are presented in Table 1, and there was no statistically significant intergroup difference in age, sex, and BMI. The mean age at the diagnosis of IIM was 48.4 years, and the mean duration of the disease was 2.24 years. Thirty-four patients (68%) presented with proximal muscle weakness, 30 (60%) had skin manifestations such as Gottron's sign, heliotrope rash, or V-neck sign, and 27 (55.1%) were diagnosed with interstitial lung disease at an initial presentation. Anti-Jo-1 antibody was identified in six patients. Forty-one patients (82%) had a previous history of glucocorticoid therapy before the enrollment date. The mean values were stated as CK of 532 U/L, LDH of 329 IU/L, and CRP of 1.44 mg/dL at the sample collection date.

Table 1. Demographics and clinical parameters of study participants.

	IIM (n = 50)	**AS (n = 30)**	**Control (n = 10)**	***p*-Value**
Age (y) *	50.7 ± 12.2	52.5 ± 11.4	45.0 ± 15.0	0.249
Male	25 (50.0)	15 (50.0)	5 (50.0)	1.000
BMI (kg/m^2)	23.5 ± 3.4	22.8 ± 2.8	25.0 ± 2.2	0.376
Age at disease onset (y)	48.4 ± 12.4			
Disease duration (y)	2.24 ± 2.74			
Clinical features at disease onset (n)				
Proximal muscle weakness	34 (68.0)			
Skin manifestations †	30 (60.0)			
Interstitial lung disease	27 (55.1)			
Elevated serum level of enzymes ‡	46 (92.0)			
Anti-Jo1 antibody present	6 (12.2)			
Laboratory data *				
WBC ($\times 10^3/\mu L$)	8445 ± 5095			
Creatinine kinase (U/L)	532 ± 934			

Aldolase (U/L)	19.1 ± 23.2
Myoglobin (ng/mL)	694 ± 885
LDH (IU/L)	329 ± 179
C-reactive protein (mg/dL)	1.44 ± 3.59
ESR (mm/h)	30.5 ± 28.1
Treatment history §	
Corticosteroids (ever)	41 (82.0)
IVIG (ever)	4 (8.0)

Note: Values are expressed as the mean ± SD or numbers (%) unless stated otherwise. * At sample col-lection date; † Gottron's sign or heliotrope rash or V-neck sign; ‡ Creatinine kinase or lactate dehydrogenase or aspartate aminotransferase or alanine aminotransferase; § Treatment history before the sample collection date; Abbreviation: ANA, Antinuclear antibodies; ESR, Erythrocyte sedimentation rate; IVIG, Intravenous immunoglobulin; LDH, Lactate dehydrogenase; WBC, White blood cell.

2. Metabolic profiling of healthy control, AS and IIM patients

High-throughput targeted metabolomics analysis was performed to explore the metabolic signature of IIM using serum samples from IIM patients, AS patients, and healthy controls. After missing value imputation, a total of 148 metabolites remained for further analysis in human serum. A full name of metabolites was shown in Table 2. Principal component analysis (PCA), an unsupervised multivariate statistical analysis, in human serum samples showed differences between the IIM group and the other groups (Figure 2), whereas the AS and healthy control groups showed no intergroup difference. In total, 88 significant metabolites were identified using ANOVA with an FDR-adjusted p-value less than 0.05 for IIM, AS, and healthy control groups (Table 3). The clustered heatmap using Euclidean distance and the Ward method, revealed distinct clusters with metabolite similarity (Figures 3A, B). The heatmap with group averages clearly showed differences between the IIM, AS, and healthy control groups (Figures 4A, B). In particular, the metabolic signature between the healthy control and IIM was distinctively different. L-acetylcarnitine, cis-5-tetradecenoylcarnitine, serotonin, glycine, creatinine and methionine were down-regulated, whereas all other significant metabolites were upregulated in IIM compared to the healthy control (Figure 4A). To

visualize the global metabolomic data, mapping of biochemical pathways and chemical similarity for significant metabolites in IIM compared to healthy controls was conducted (Figure 5). All significant metabolites were mapped as three main clusters: (i) amino acids and biogenic amine, (ii) glycerophospholipids, and acylcarnitine, and (iii) sphingomyelin. Clearly, all significantly changed sphingomyelins were down-regulated in IIM compared to the healthy controls. Besides sphingomyelin, numerous metabolites in other clusters were altered in the serum of IIM compared to healthy controls. These results support that inflammation in muscle impacts the systemic serum metabolite profile.

Table 2. Abbreviations used to describe metabolites.

Metabolite abbreviation	Full name	HMDB ID
Ala	L-Alanine	HMDB0000161
Arg	L-Arginine	HMDB0000517
Asn	L-Asparagine	HMDB0000168
Asp	L-Aspartic acid	HMDB0000191
Cit	Citrulline	HMDB0000904
Gln	L-Glutamine	HMDB0000641
Glu	L-Glutamic acid	HMDB0000148
Gly	Glycine	HMDB0000123
His	L-Histidine	HMDB0000177
Ile	L-Isoleucine	HMDB0000172
Leu	L-Leucine	HMDB0000687
Lys	L-Lysine	HMDB0000182
Met	L-Methionine	HMDB0000696
Orn	Ornithine	HMDB0000214
Phe	L-Phenylalanine	HMDB0000159

Pro	L-Proline	HMDB0000162
Ser	L-Serine	HMDB0000187
Thr	L-Threonine	HMDB0000167
Trp	L-Tryptophan	HMDB0000929
Tyr	L-Tyrosine	HMDB0000158
Val	L-Valine	HMDB0000883
Ac-Orn	N-Acetylornithine	HMDB0003357
ADMA	Asymmetric dimethylarginine	HMDB0001539
alpha-AAA	Aminoadipic acid	HMDB0000510
c4-OH-Pro	cis-4-Hydroxyproline	HMDB0240251
Carnosine	Carnosine	HMDB0000033
Creatinine	Creatinine	HMDB0000562
DOPA	L-Dopa	HMDB0000181
Dopamine	Dopamine	HMDB0000073
Histamine	Histamine	HMDB0000870
Kynurenine	L-Kynurenine	HMDB0000684
Met-SO	Methionine sulfoxide	HMDB0002005

Nitro-Tyr	3-Nitrotyrosine	HMDB0001904
PEA	Phenylethylamine	HMDB0012275
Putrescine	Putrescine	HMDB0001414
SDMA	Symmetric dimethylarginine	HMDB0003334
Serotonin	Serotonin	HMDB0000259
Spermidine	Spermidine	HMDB0001257
Spermine	Spermine	HMDB0001256
t4-OH-Pro	4-Hydroxyproline	HMDB0000725
Taurine	Taurine	HMDB0000251

Table 3. List of significant metabolites in serum of IIM patients, AS patients, and healthy controls.

Metabolites	FDR-adjusted p-value
Met-SO	4.49E-06
PC aa C38:4	1.55E-05
Glu	3.55E-05
PC ae C38:0	8.07E-05
PC aa C38:6	8.07E-05
PC aa C38:1	8.07E-05
PC ae C36:1	8.07E-05
PC aa C42:4	8.58E-05
PC ae C38:6	8.58E-05
PC aa C40:6	8.58E-05
PC aa C24:0	0.0001
lysoPC a C24:0	0.0002
PC ae C38:2	0.0002
PC ae C38:5	0.0002
PC aa C36:4	0.0003
Gln	0.0003
Kynurenine	0.0003
C2	0.0003
PC ae C36:5	0.0003
PC aa C38:5	0.0003
PC aa C42:5	0.0005
PC aa C36:0	0.0005
PC ae C42:4	0.0006
PC ae C40:5	0.0006
PC aa C40:3	0.0006
lysoPC a C26:0	0.0006

PC aa C42:2	0.0009
PC ae C30:2	0.0009
Serotonin	0.0010
Asp	0.0011
PC aa C40:1	0.0011
PC aa C40:2	0.0021
Met	0.0022
Phe	0.0024
lysoPC a C20:4	0.0026
PC ae C42:5	0.0026
PC ae C40:6	0.0026
Ile	0.0026
Ala	0.0026
Leu	0.0026
PC ae C44:3	0.0026
Ser	0.0027
ADMA	0.0027
PC ae C44:4	0.0027
SM C26:0	0.0037
Pro	0.0039
SM (OH) C22:2	0.0040
PC ae C36:4	0.0040
C14:1	0.0040
lysoPC a C28:0	0.0040
lysoPC a C17:0	0.0041
Orn	0.0041
PC ae C30:0	0.0042
PC aa C42:1	0.0042
PC ae C40:2	0.0042

Lys	0.0042
PC ae C38:3	0.0042
PC ae C42:3	0.0043
PC aa C30:2	0.0043
lysoPC a C28:1	0.0043
PC aa C40:4	0.0052
Val	0.0057
SM (OH) C22:1	0.0061
PC ae C40:4	0.0063
PC aa C38:3	0.0077
PC ae C30:1	0.0094
Creatinine	0.0100
Taurine	0.0112
Tyr	0.0112
Gly	0.0135
PC ae C38:0	0.0151
lysoPC a C16:0	0.0151
alpha-AAA	0.0151
PC ae C40:3	0.0169
SM (OH) C24:1	0.0170
Putrescine	0.0173
PC ae C36:2	0.0173
PC ae C42:1	0.0179
PC aa C40:5	0.0183
PC ae C42:2	0.0232
PC aa C32:0	0.0308
PC aa C42:6	0.0330
t4-OH-Pro	0.0333
lysoPC a C18:0	0.0361

lysoPC a C16:1	0.0422
SM (OH) C14:1	0.0430
PC aa C36:3	0.0439
PC ae C36:0	0.0439

Statistical analysis was performed using one-way analysis of variance (ANOVA).

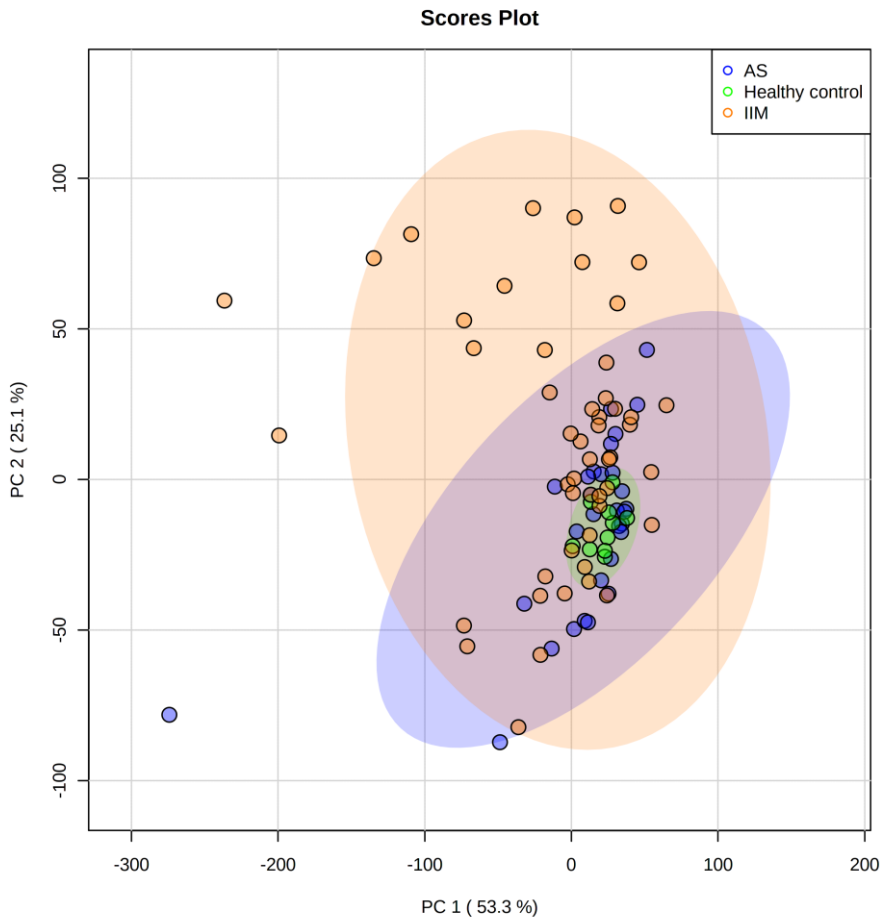

Figure 2. Metabolites distribution of AS patients, IIM patients, and healthy controls by PCA plot.

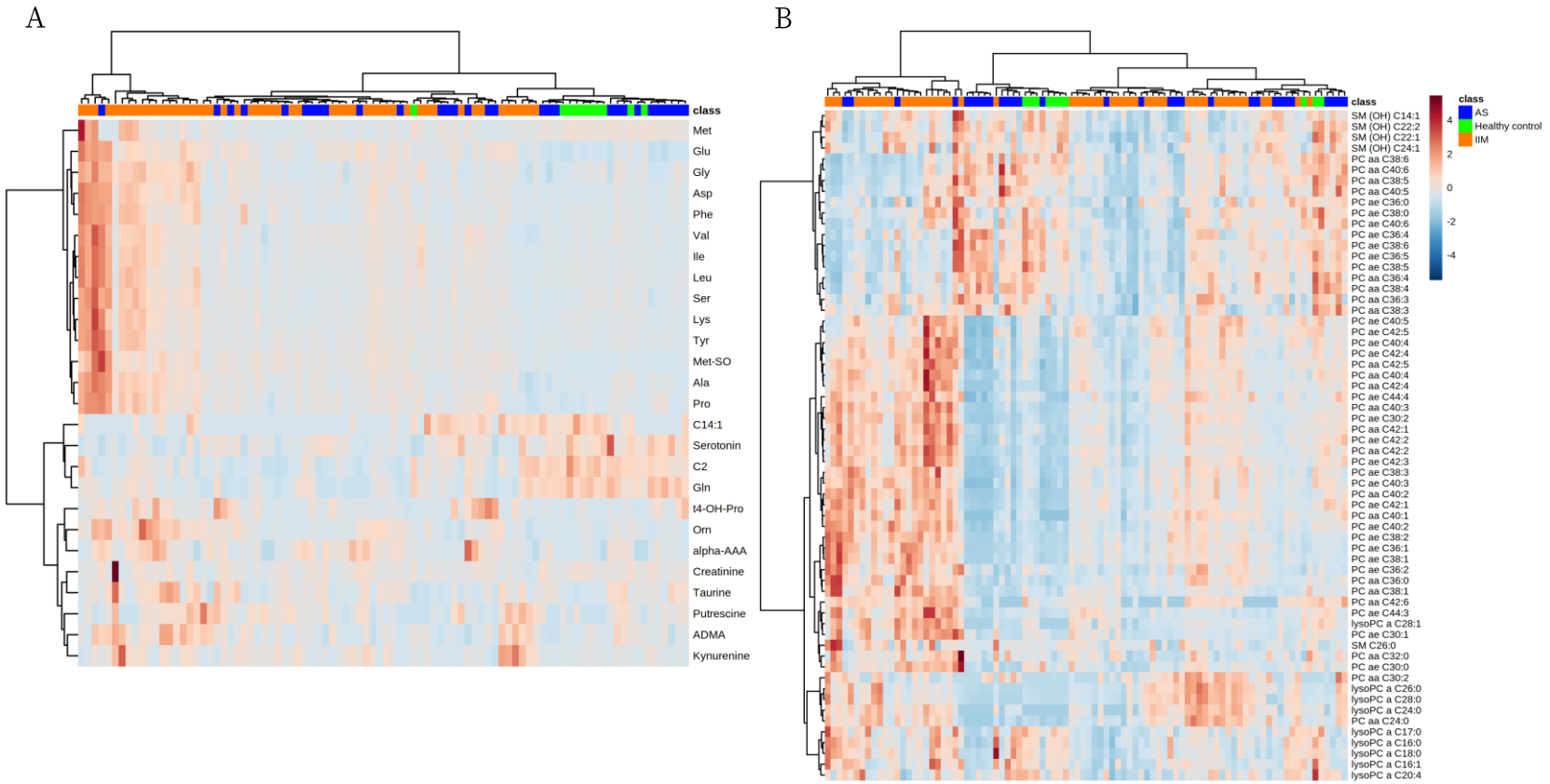

Figure 3. Cluster heatmap of significant metabolites in serum of AS patients, IIM patients, and healthy controls.

(A) including amino acid, biogenic amine and acylcarnitine class. (B) including SMs, lysoPCs, PC, and hexoses.

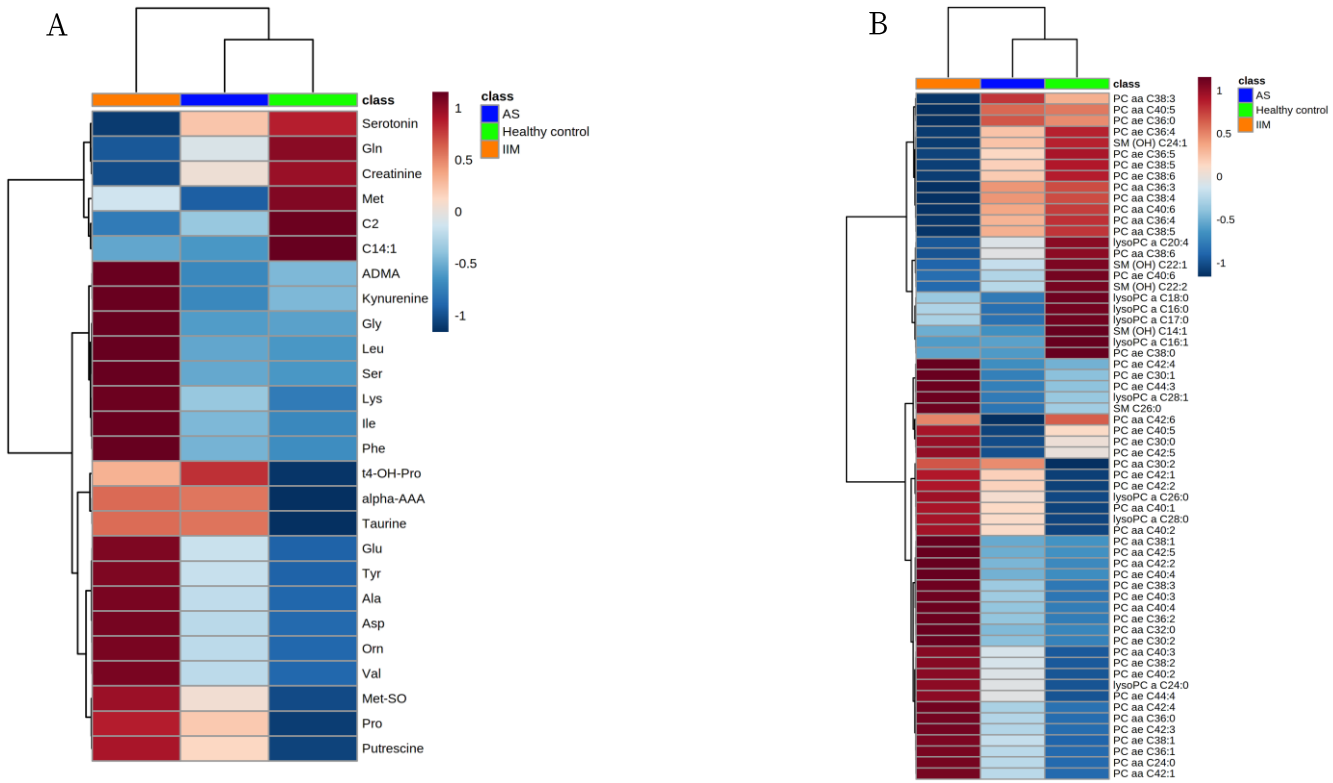

Figure 4. Group averaged heatmap of significant metabolites in serum of AS patients, IIM patients, and healthy controls.

(A) including amino acid, biogenic amine and acylcarnitine class. (B) including SMs, lysoPCs, PC, and hexoses.

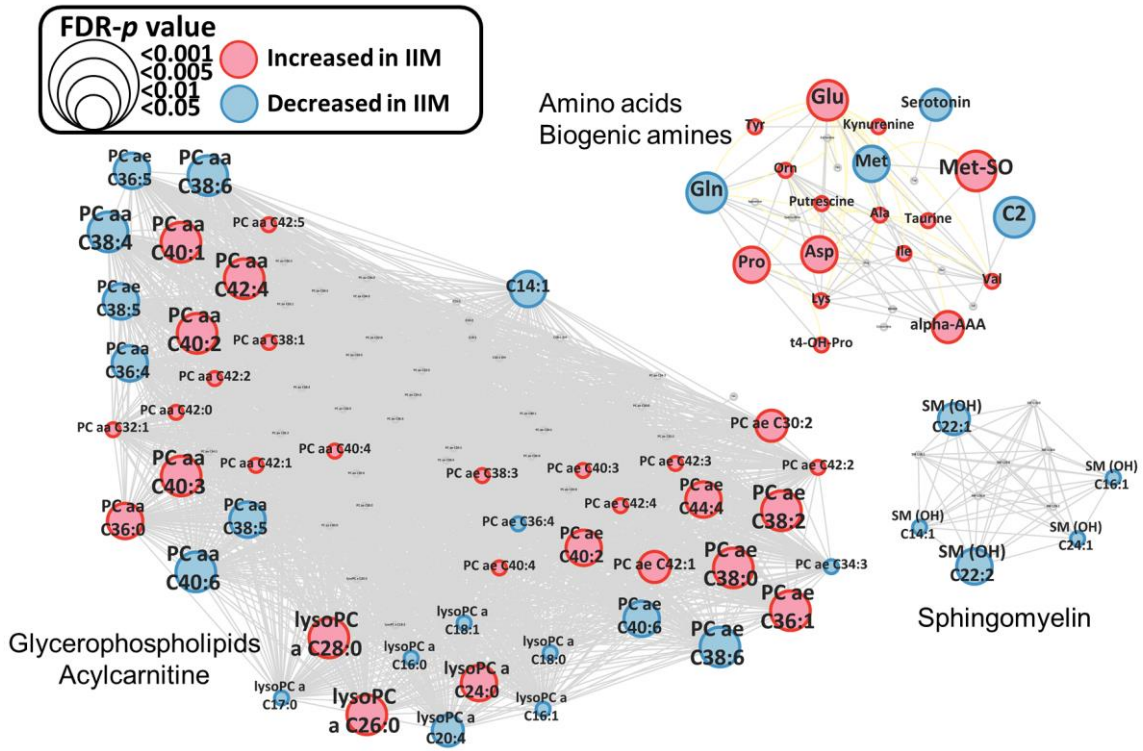

Figure 5. MetaMapp metabolomic networks of human serum alterations in IIM patients compared to healthy controls.

Border color and node color: red indicates up-regulation in IIM, and blue indicates down-regulation in IIM. Node size indicates the FDR-adjusted p-value.

3. Predictive Biomarker and Machine Learning Algorithm Optimization for Distinguishing IIM

Following the ANOVA test, multiple comparisons were performed to identify 37 IIM-specific metabolites (Table 4 and Figure 6). Among these, a combination of seven metabolites was calculated to distinguish IIM from AS and healthy controls using backward stepwise selection (Figure 7). LR, RF, and SVM algorithms were used to establish a prediction model for IIM. ROC analysis using LR, RF, and SVM was performed to assess model performance, yielding area under the ROC curve (AUC) values of 0.966 (95% CI, 0.928–1.000), 1 (1.000–1.000), and 0.957 (0.910–1.000), respectively (Figure 8A). The prediction model was evaluated using a five-fold cross-validation method, resulting in AUC values were 0.955 (LR), 0.908 (RF) and 0.918 (SVM) (Figure 8B). By using the prediction model as well as 5-fold cross-validation, a panel of seven metabolite was identified as powerful contributors in distinguishing IIM from the other groups (Figure 8B).

Table 4. List of IIM specific metabolites based on ANOVA and post-hoc analysis.

Metabolite	IIM	AS	Healthy control	ANOVA (FDR-adjusted p-value)	Post-hoc analysis
Ala	723.84±46.99	566.23±43.33	480.5±36.72	0.0026	**, †
Asp	157.89±19.58	82.03±14.32	44.66±3.84	0.0011	***, †
Glu	650.62±46.49	397.02±51.95	242.4±33.14	0.0000	****, † † †
Orn	224.1±16.49	162.05±11.65	130.57±9.14	0.0041	**, †
Val	406.22±26.74	330.53±24.58	291.9±12.19	0.0057	*, †
Met-SO	39.36±4.47	22.42±7.25	2.3±0.44	0.0000	****, † † †
Serotonin	0.31±0.02	0.48±0.05	0.56±0.08	0.0010	**, † †
lysoPC a C20:4	4.54±0.23	5.53±0.28	6.75±0.72	0.0026	**, †
lysoPC a C24:0	0.53±0.03	0.33±0.04	0.16±0.05	0.0002	***, † †
lysoPC a C26:0	0.76±0.08	0.5±0.09	0.16±0.03	0.0006	***, †
PC aa C24:0	0.31±0.02	0.17±0.02	0.1±0.02	0.0001	***, † † †
PC aa C36:0	6.84±0.46	4.68±0.4	3.72±0.39	0.0005	**, † †
PC aa C36:4	76.98±3.22	102.41±5.25	111.26±9.39	0.0003	**, † † †
PC aa C38:1	4.68±0.37	2.54±0.42	2.4±0.37	0.0001	*, † † † †

PC aa C38:4	41.43±1.71	64.67±3.91	68.59±6.37	0.0000	***, † † † †
PC aa C38:5	24.48±1.35	36.09±2.74	39.76±3.87	0.0003	**, † † †
PC aa C38:6	48.14±2.57	67±5.12	88.33±4.36	0.0001	****, † †
PC aa C40:3	2.46±0.16	1.68±0.18	1.11±0.16	0.0006	***, †
PC aa C40:4	4.94±0.26	3.75±0.25	3.44±0.47	0.0052	*, † †
PC aa C40:6	18.82±1.09	29.84±2.68	32.73±1.76	0.0001	***, † † †
PC aa C42:1	0.48±0.03	0.37±0.03	0.32±0.03	0.0042	*, †
PC aa C42:2	0.9±0.05	0.59±0.05	0.55±0.07	0.0009	*, † † †
PC aa C42:4	1.3±0.08	0.79±0.08	0.59±0.1	0.0001	***, † † †
PC aa C42:5	0.73±0.03	0.52±0.04	0.5±0.06	0.0005	*, † † †
PC ae C30:2	0.25±0.01	0.16±0.02	0.14±0.02	0.0009	**, † †
PC ae C36:1	22.43±1.44	13.97±1.5	9.73±0.85	0.0001	***, † † †
PC ae C36:4	8.55±0.49	11.1±0.8	12.3±1.04	0.0040	**, †
PC ae C36:5	5.53±0.31	7.55±0.5	8.86±0.77	0.0003	***, † †
PC ae C38:0	9.63±0.77	5.43±0.82	3.01±0.44	0.0001	****, † † †
PC ae C38:2	9.41±0.64	6.12±0.82	3.68±0.47	0.0002	***, † †
PC ae C38:3	13.71±0.77	9.76±1.1	8.55±1.37	0.0042	*, † †

PC ae C38:5	7.22±0.37	9.94±0.65	11.52±1.12	0.0002	**, † † †
PC ae C38:6	3.9±0.25	5.71±0.47	6.66±0.4	0.0001	***, † † †
PC ae C42:3	1.85±0.09	1.4±0.11	1.21±0.14	0.0043	*, †
PC ae C42:4	1.76±0.08	1.23±0.09	1.29±0.15	0.0006	*, † † †
PC ae C44:4	0.53±0.02	0.44±0.02	0.36±0.03	0.0027	**, †
SM (OH) C24:1	0.95±0.04	1.08±0.05	1.15±0.08	0.0170	*, †

Concentration of each group represented as mean ± SEM. Comparing Healthy control vs IIM, * $p < 0.05$; ** $p < 0.005$; *** $p < 0.0005$, *** $p < 0.0001$. Comparing AS vs IIM, † $p < 0.05$; † † $p < 0.005$; † † † $p < 0.0005$, † † † † $p < 0.0001$. Listed metabolites were not significantly different between healthy control and AS.

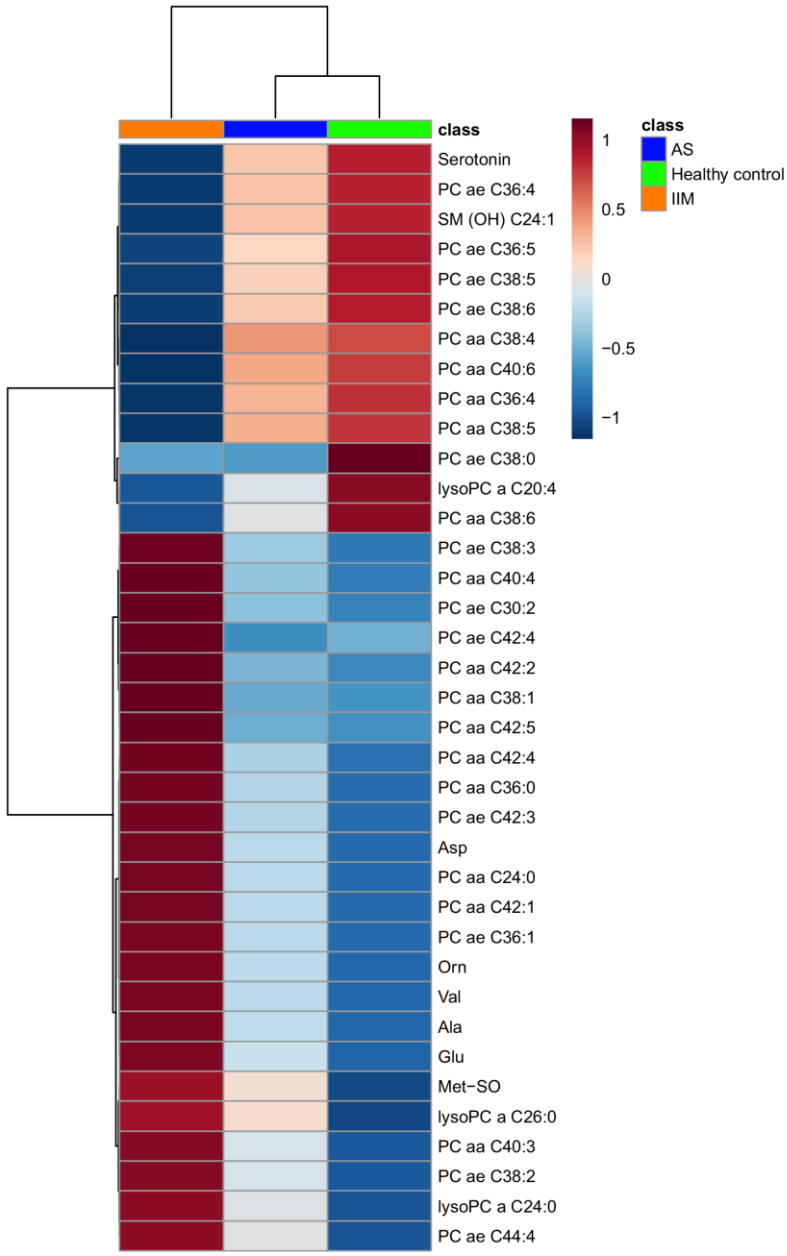

Figure 6. Heatmap of IIM-specific metabolites based on ANOVA and post-hoc analysis.

IIM Specific metabolites were selected using FDR adjusted p-value < 0.05 by Kruskal-Wallis test and post-hoc analysis by Dunn's test between three groups.

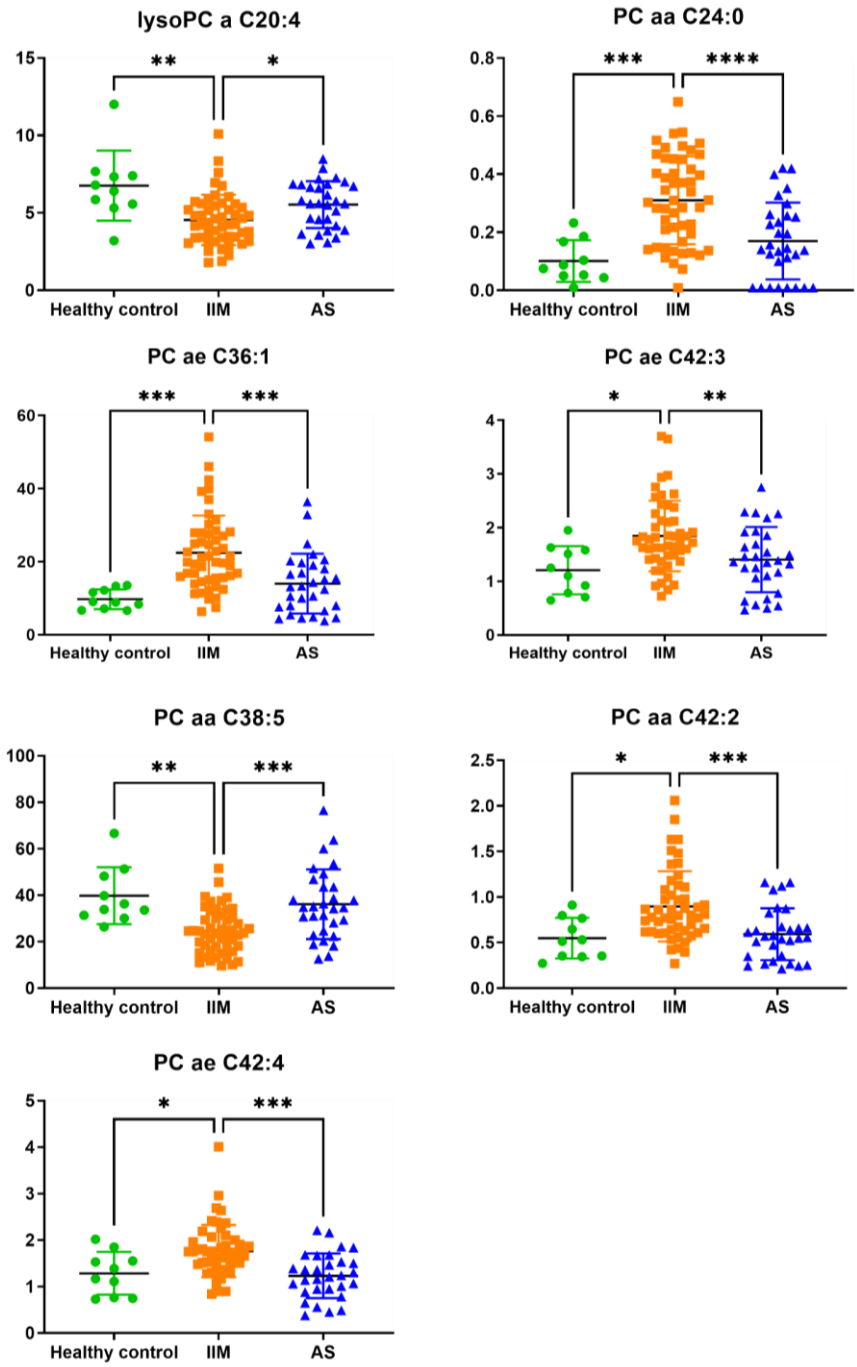

Figure 7. The individual plot of IIM-specific metabolites.

IIM-specific metabolites were selected by the backward stepwise method for constructing a prediction model. Horizontal line indicates concentration levels. * p <0.05; ** p < 0.005; *** p < 0.0005, and **** p < 0.0001.

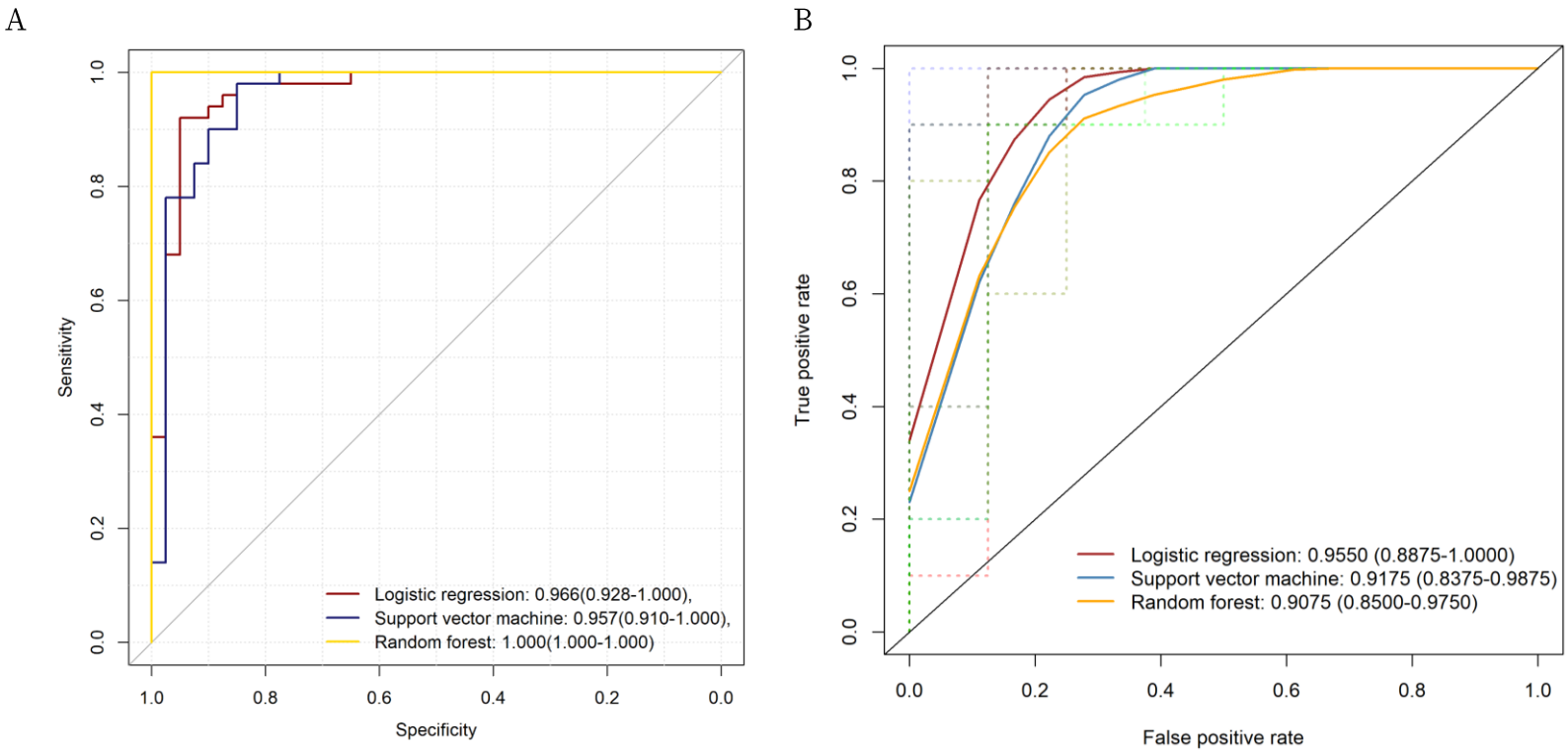

Figure 8. ROC curves and AUC values of a set of 7 metabolites panel.

(A) prediction model for discriminating IIM patients. (B) five-fold cross-validation. AUC values were calculated for each machine learning method; red indicates logistic regression, blue indicates support vector machine, and yellow indicates random forest.

4. Bile acid levels in human serum

After missing value imputation, a total of 15 bile acids remained for further analysis in human serum. The concentration of serum bile acids levels was measured in IIM patients, AS patients, and healthy controls. PCA based on serum bile acid characteristics showed no significant differences between the three groups (Figure 9A). In addition, there was no IIM specific bile acid from AS and healthy control group. Hierarchical clustering heatmap also revealed no distinct variation among these groups (Figure 9B). Even though, there was no IIM specific bile acid, GCA, GCDCA, TCA, TCDCA and TUDCA were significantly changed in IIM compared to healthy controls (Figure 10). GCDCA, GUDCA, TCDCA and TUDCA were also significantly changed in AS compared to healthy control (Figure 10).

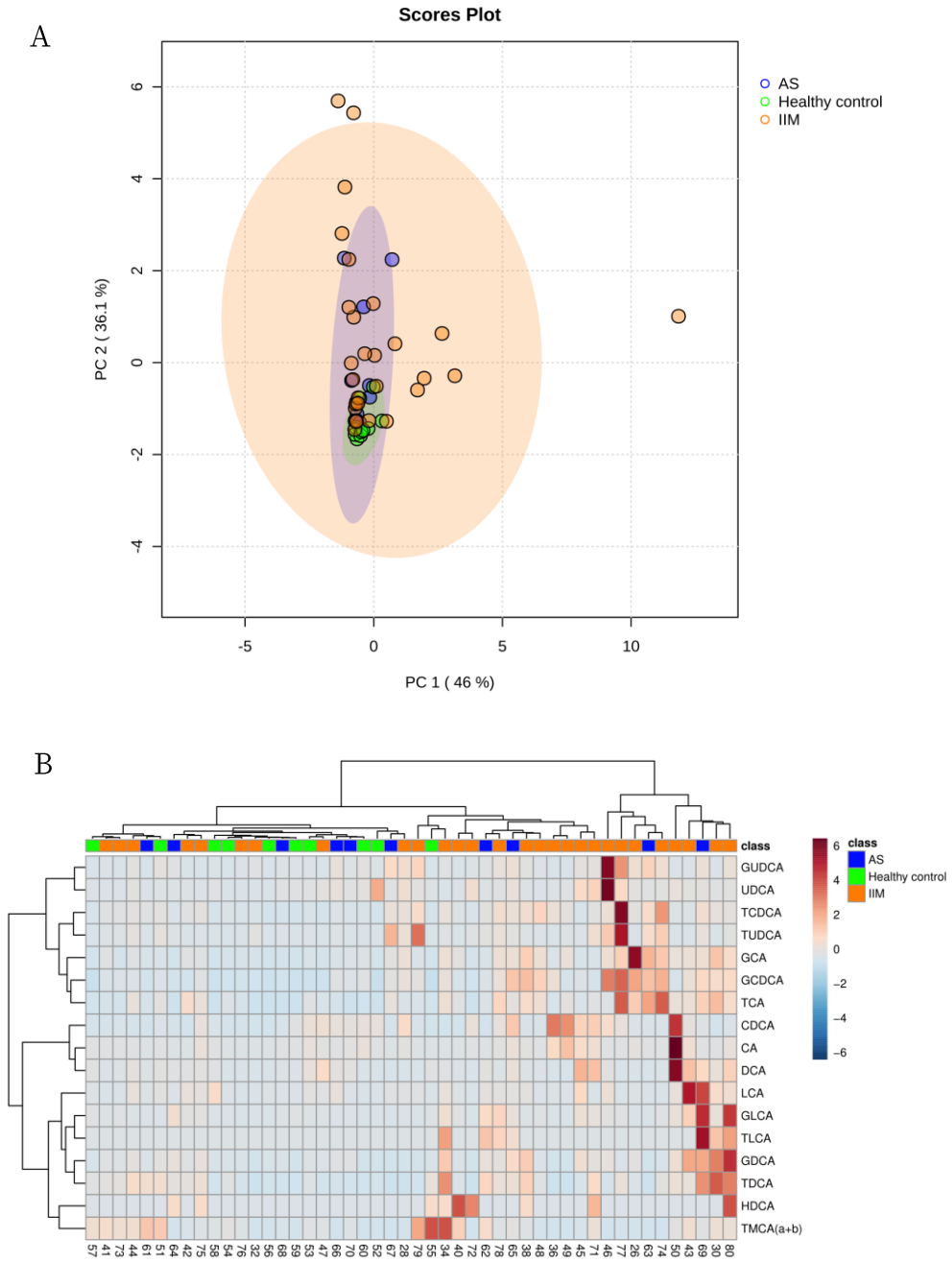

Figure 9. Multivariate analysis of bile acids in serum samples.

(A) The bile acids distribution of AS patients, IIM patients, and healthy controls by PCA score plot showing relatively high within group variation in IIM group. (B) Cluster heatmap of bile acids in all individual samples.

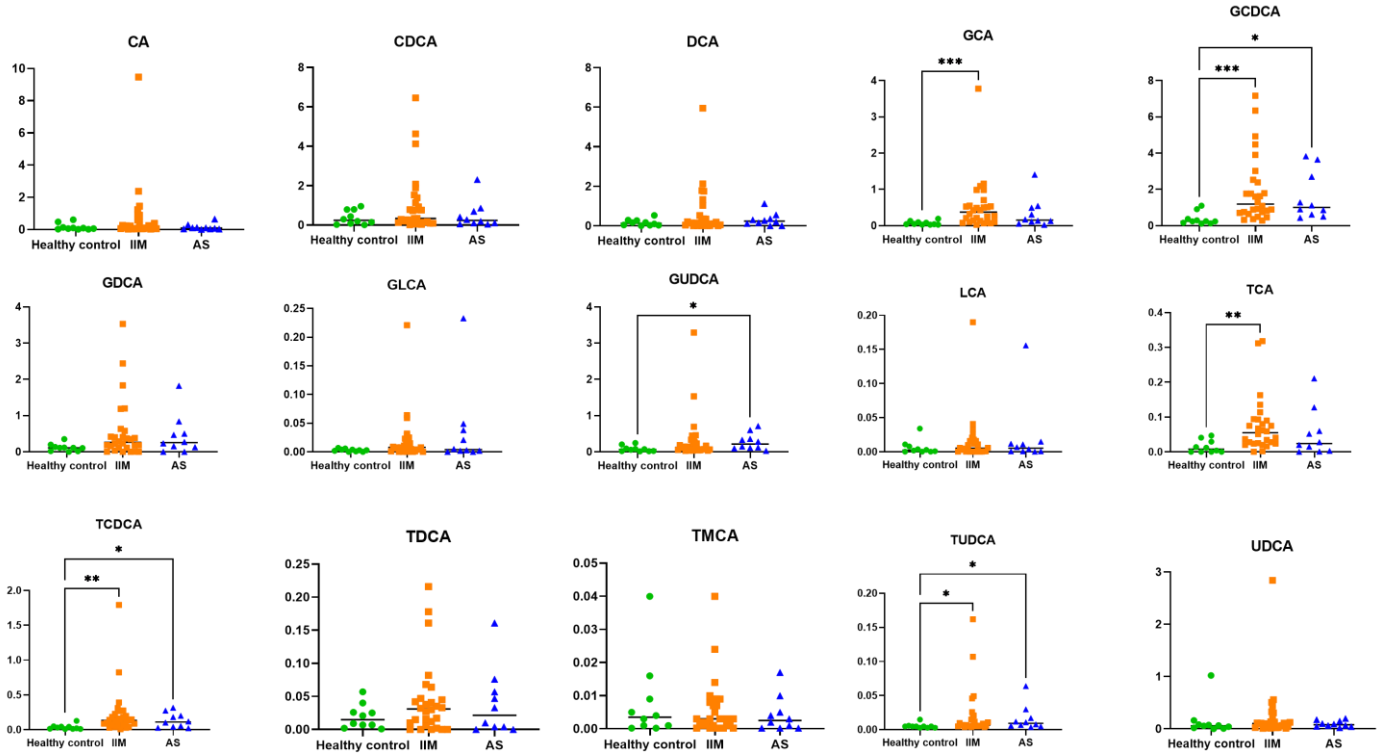

Figure 10. Individual scatter plots of bile acids in human serum sample of IIM patients, AS patients, and healthy control based on ANOVA and post-hoc analysis.

Horizontal line indicates concentration levels. Significance was indicated with *. (* $p < 0.05$).

5. Oxylipin profiles from untargeted metabolomic analysis

Serum samples of 28 patients with IIM, 10 patients with AS, and 10 healthy controls were subjected to untargeted analysis. A total of 3042 metabolic features were detected in the ESI^+ and ESI^- mode. Pooled QC samples were closely clustered in the center of the PCA model, validating the stability of this study. As demonstrated by the PCA in Figure 11, serum metabolome showed clear differences between the healthy control group and disease groups in both positive (ESI^+) and negative (ESI^-) electrospray ionization mode. The similarity in serum metabolomes between IIM and AS groups indicated that inflammation status may share a number of metabolic features. A total of 796 metabolites were significantly changed in IIM compared to healthy control. Further evaluation using ANOVA revealed that a total of 241 metabolites were significantly changed in IIM compared to AS and healthy controls (Figure 12). Finally, 40 metabolites were annotated from a public library, and 8 metabolites were identified using authentic compounds (Figure 13). Except for L-methionine, the IIM specific metabolites were upregulated in the IIM group compared to the healthy control and AS group (Figure 13). The majority of these metabolites, 6 out of 8, were oxylipins that mediate oxidative stress and inflammation.

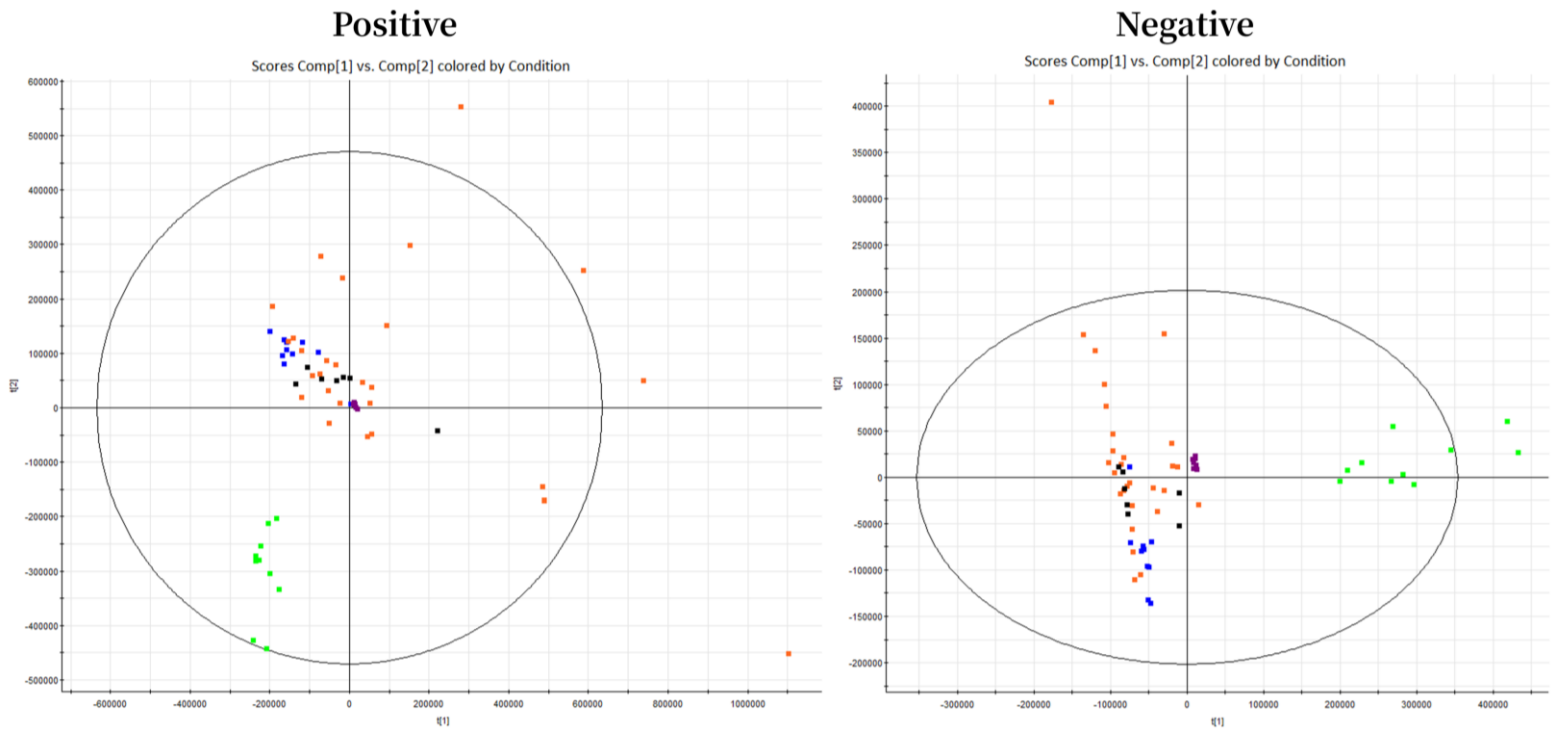

Figure 11. PCA plot of AS patients, IIM patients, and healthy controls in positive and negative mode.

Color codes are QC: purple, Healthy control: green, AS: blue, IIM: orange, IIM follow up: black.

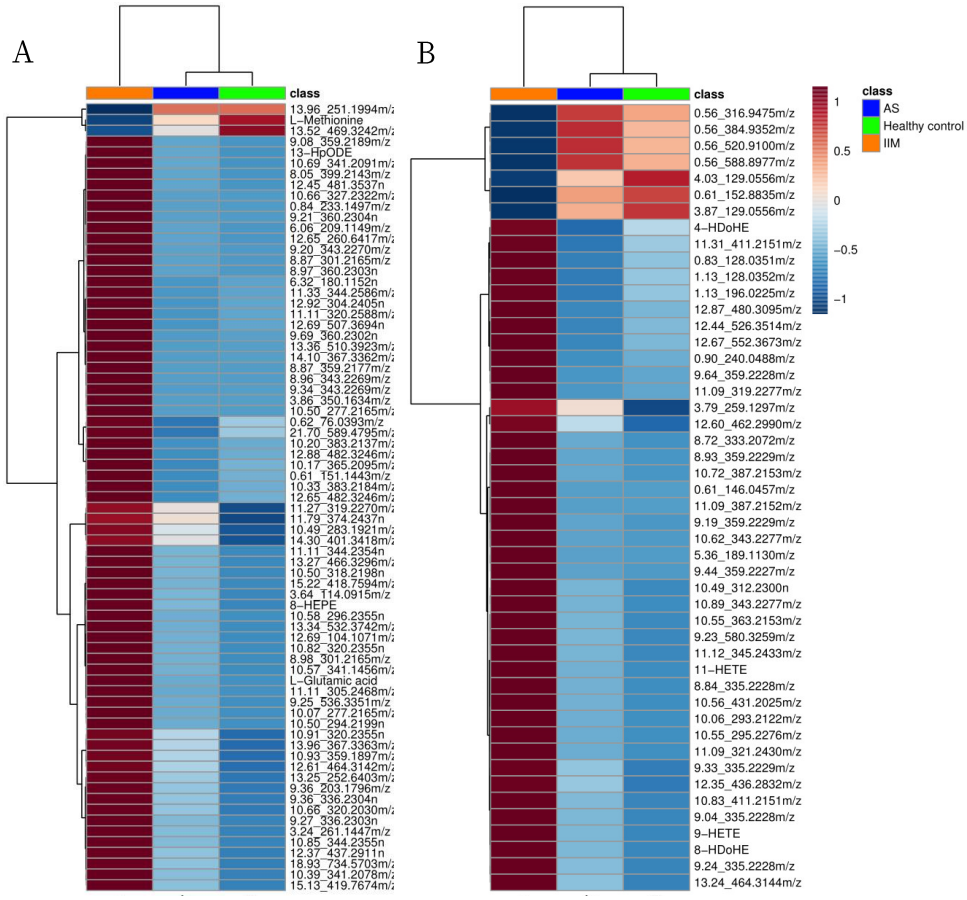

Figure 12. Heatmap of significant metabolites based on ANOVA from untargeted metabolomics data.

(A) Positive mode. (B) Negative mode.

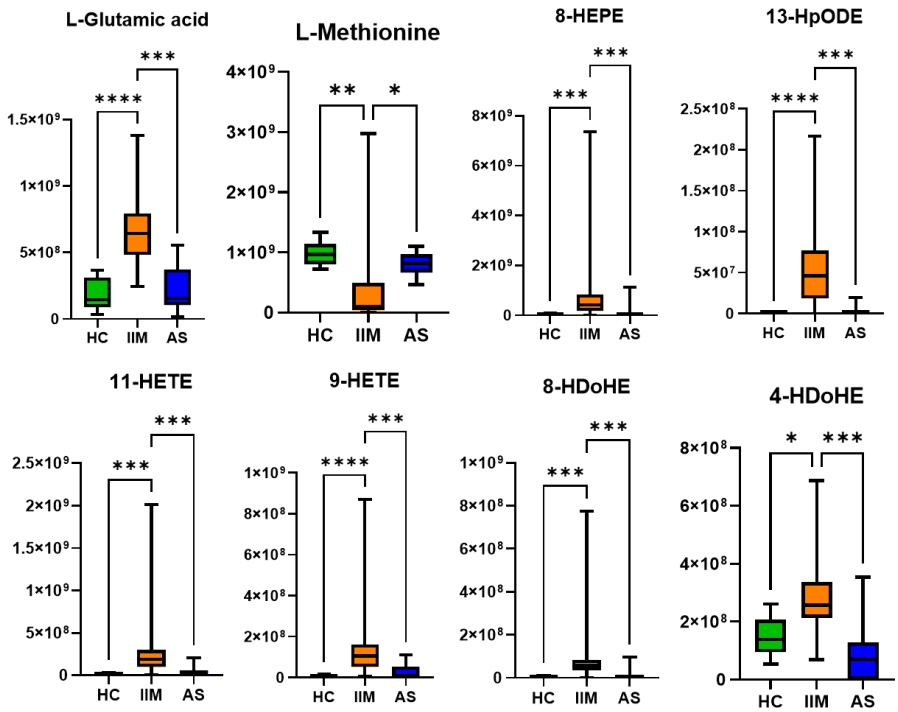

Figure 13. The individual box plots of IIM specific metabolites in serum samples of IIM patients, AS patients, and healthy control.

Horizontal line indicates relative intensity. Significance was indicated with *. * p <0.05; ** p < 0.005; *** p < 0.0005, and **** p < 0.0001

6. Serum metabolites change after corticosteroid treatment

Among the participants of our study, the majority of patients (82%) received corticosteroid treatment. We collected pre-dose and post-dose data of corticosteroid treatment from 7 patients. PCAs, using both targeted and untargeted metabolomics data, did not show clear separation between the pre- and post-treatment (follow-up) groups (Figure 14). Furthermore, we identified 7 metabolites with raw p-values < 0.05 from the Wilcoxon test. Among these metabolites, four oxylipins and Met-SO demonstrated a decrease in levels during the follow-up period, while C2 and serotonin showed an increase (Figure 15). The metabolic profile following corticosteroid treatment in IIM patients exhibits a resemblance to that of healthy controls, contrasting with the metabolic profile observed in IIM patients prior to treatment.

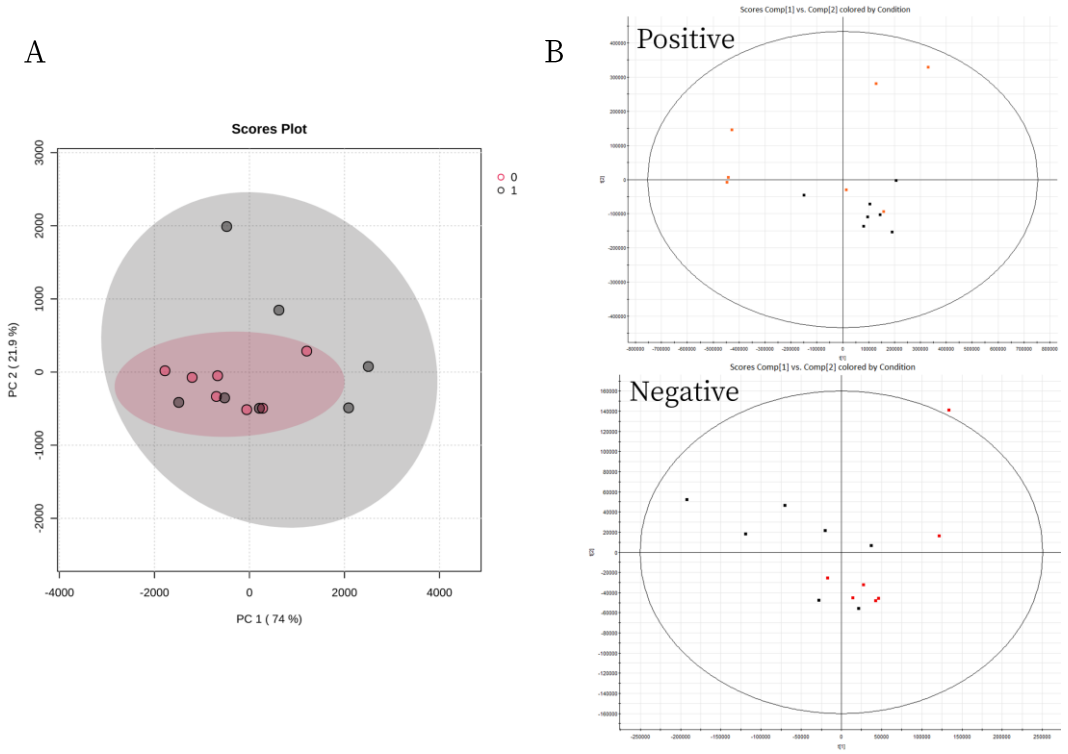

Figure 14. PCA plot of IIM patients and paired samples after treatment of corticosteroids.

(A) Targeted metabolomics including 188 metabolites. (B) Untargeted metabolomics with global profile in both ionization mode. Black dots indicate IIM serum samples before treatment. Red dots indicate IIM serum samples after treatment (IIM follow-up).

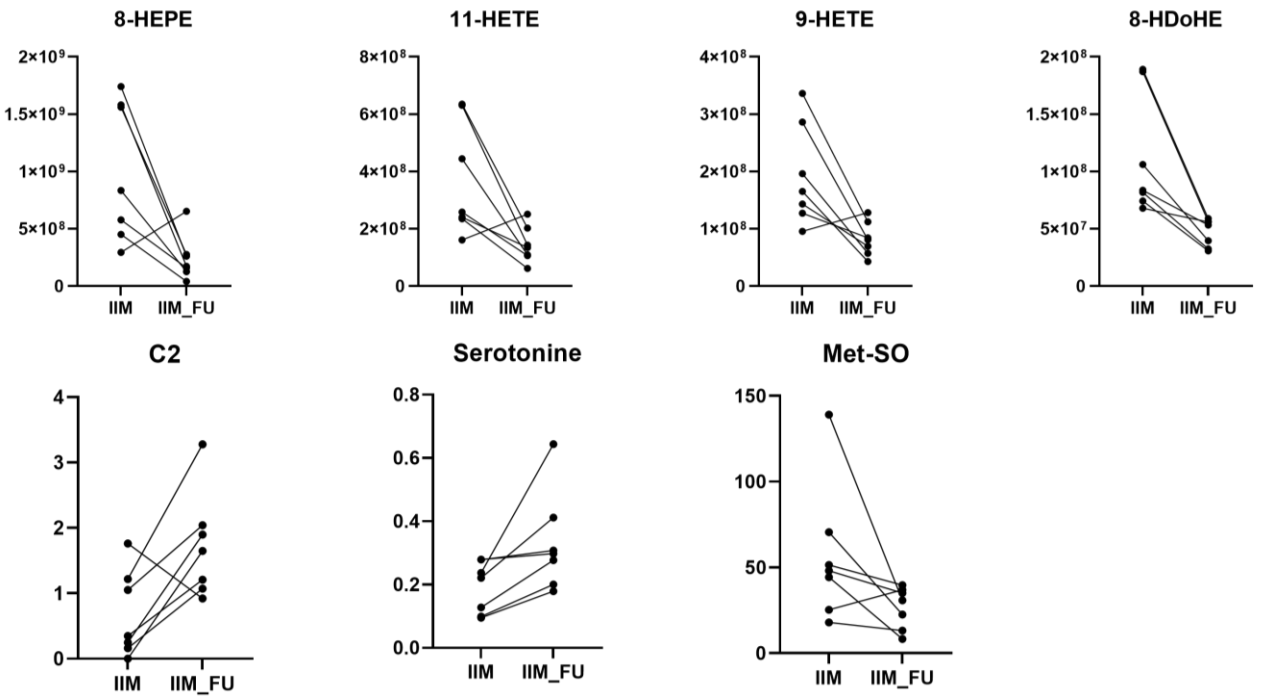

Figure 15. The individual spaghetti plot of metabolites with raw p-value <0.05 from both targeted and untargeted data.

IIM indicates serum samples of IIM patients before treatment. IIM_FU indicates serum samples of IIM patients after treatment.

7. Metabolic profiling in the C-protein-induced myositis mouse model

To examine the alteration of metabolites in the muscle, we used a mouse model induced by injection of immunogens. Mouse quadriceps and hamstring muscles were stained with hematoxylin and eosin (H&E) to assess muscle histology (Figure 16A). The histological score showed a significant increase in the quadriceps and hamstring muscles of CIM mice compared to control mice (Figure 16B). CIM mice showed increased production of cytokines TNF-α, IL-6, and IL-1 in mouse serum samples (Figure 16C). Univariate and multivariate analyses were performed to explore the effect on the metabolite profile in muscle tissue with inflammation. After missing value imputation, a total of 157 metabolites remained for further analysis in mouse muscle tissue. PCA analysis of mouse muscle samples showed a difference between CIM and control mice (Figure 17A). A volcano plot was constructed to visualize significant metabolites (t-test with FDR-adjusted *p*-value less than 0.05) between CIM and control mice. (Figure 17B). In total, 68 metabolites were changed in the tissue of CIM mice (Table 5). A clustered heatmap showed the similarity of the metabolite patterns of individual samples in each group (Figure 17C). Among the significant metabolites, the levels of amino acids, biogenic amines, and acylcarnitines, except taurine, were decreased in CIM

mice.Conversely, the levels of all lipids increased in CIM mice. Interestingly, biogenic amines, except taurine, and all metabolites from other classes showed the same pattern in CIM mice in the network analysis (Figure 18). In addition, 37 metabolites were altered in the serum of CIM mice compared to controls (Figures 19, 20 and Table 6). Significant metabolites such as carnosine, tryptophan, and creatinine observed in CIM mouse muscle, were also altered in the serum of CIM mice (Figure 20).

Table 5. List of significant metabolites in mouse tissue.

Metabolites	Fold change	FDR-adjusted p-value
PC ae C36:2	3.1	0.0122
PC ae C34:2	3.1	0.0122
PC ae C36:3	3.0	0.0122
PC aa C34:3	2.8	0.0122
PC aa C36:2	3.5	0.0139
PC aa C34:2	2.4	0.0139
Creatinine	0.5	0.0139
PC aa C36:1	3.5	0.0171
PC aa C40:4	3.2	0.0171
PC aa C32:0	2.9	0.0171
PC ae C34:3	2.8	0.0171
PC aa C34:1	2.6	0.0171
PC aa C32:2	2.6	0.0171
PC ae C34:1	2.6	0.0171
PC ae C38:5	2.5	0.0171
PC ae C36:4	2.3	0.0171
SM C16:0	2.1	0.0171
Carnosine	0.5	0.0171
C0	0.5	0.0171
SM (OH) C24:1	1.7	0.0171
PC ae C36:5	3.1	0.0195
PC aa C40:5	3.1	0.0195
PC aa C36:3	2.7	0.0195
PC aa C36:0	2.6	0.0195
PC ae C32:1	2.4	0.0195
PC ae C36:1	2.4	0.0195

PC aa C32:1	2.3	0.0195
C18:1	0.5	0.0195
PC ae C30:1	1.8	0.0195
Taurine	1.1	0.0195
C18:1-OH	0.6	0.0228
C16:1	0.4	0.0238
PC aa C38:4	2.5	0.0238
PC ae C38:2	2.4	0.0238
PC ae C34:0	2.3	0.0238
PC aa C38:1	2.2	0.0238
PC ae C32:2	2.2	0.0238
PC aa C42:4	1.9	0.0238
SM (OH) C16:1	1.8	0.0238
PC aa C38:0	2.5	0.0255
PC aa C40:2	2.5	0.0283
C18:2	0.3	0.0293
SM C24:1	2.8	0.0293
SM (OH) C22:1	2.7	0.0293
PC aa C38:3	2.4	0.0293
PC aa C40:6	2.4	0.0293
PC ae C38:6	2.2	0.0293
PC ae C42:1	2.0	0.0293
Met	0.7	0.0293
Tyr	0.7	0.0293
PC ae C30:0	3.0	0.0313
PC aa C30:2	1.6	0.0359
Asp	0.4	0.0364
PC aa C42:5	1.9	0.0364
PC ae C36:0	1.8	0.0364

Spermine	0.3	0.0372
Spermidine	0.5	0.0372
PC ae C38:4	1.9	0.0372
His	0.6	0.0372
SM (OH) C22:2	2.3	0.0460
SM C24:0	2.8	0.0474
C14:1	0.5	0.0474
SM (OH) C14:1	1.9	0.0474
C16:1-OH	0.6	0.0474
PC ae C38:0	1.6	0.0474
C2	0.6	0.0474
Thr	0.7	0.0474
PC ae C40:4	1.3	0.0474

Statistical analysis was performed using t-test.

Table 6. List of significant metabolites in mouse serum.

Metabolites	Fold change	FDR-adjusted p-value
lysoPC a C20:4	0.3	3.E-05
lysoPC a C20:3	0.5	0.0002
t4-OH-Pro	1.7	0.0004
Trp	0.6	0.0005
lysoPC a C17:0	0.6	0.0007
PC ae C34:1	1.5	0.0007
lysoPC a C18:2	0.5	0.0007
Carnosine	0.3	0.0007
lysoPC a C18:1	0.6	0.0010
lysoPC a C16:0	0.7	0.0012
Arg	1.7	0.0012
PC aa C40:2	1.8	0.0016
lysoPC a C16:1	0.7	0.0034
H1	0.6	0.0036
PC aa C42:4	1.6	0.0038
PC ae C40:1	0.6	0.0038
lysoPC a C18:0	0.7	0.0038
ADMA	1.6	0.0043
PC aa C36:0	0.7	0.0049
SM C26:0	0.6	0.0067
PC ae C38:0	0.7	0.0078
PC ae C36:5	0.7	0.0093
SM C18:0	0.7	0.0110
PC aa C32:1	1.5	0.0175
PC aa C30:0	1.2	0.0184
SM C16:0	1.3	0.0216
SM C24:1	1.3	0.0216

PC ae C32:1	1.3	0.0244
PC aa C36:6	0.8	0.0277
lysoPC a C24:0	0.6	0.0279
PC aa C36:4	0.6	0.0279
SM C18:1	0.7	0.0344
PC ae C42:3	0.7	0.0458
C0	0.8	0.0458
Creatinine	0.8	0.0458
SM (OH) C22:2	0.8	0.0458
PC aa C38:4	0.6	0.0488

Statistical analysis was performed using t-test.

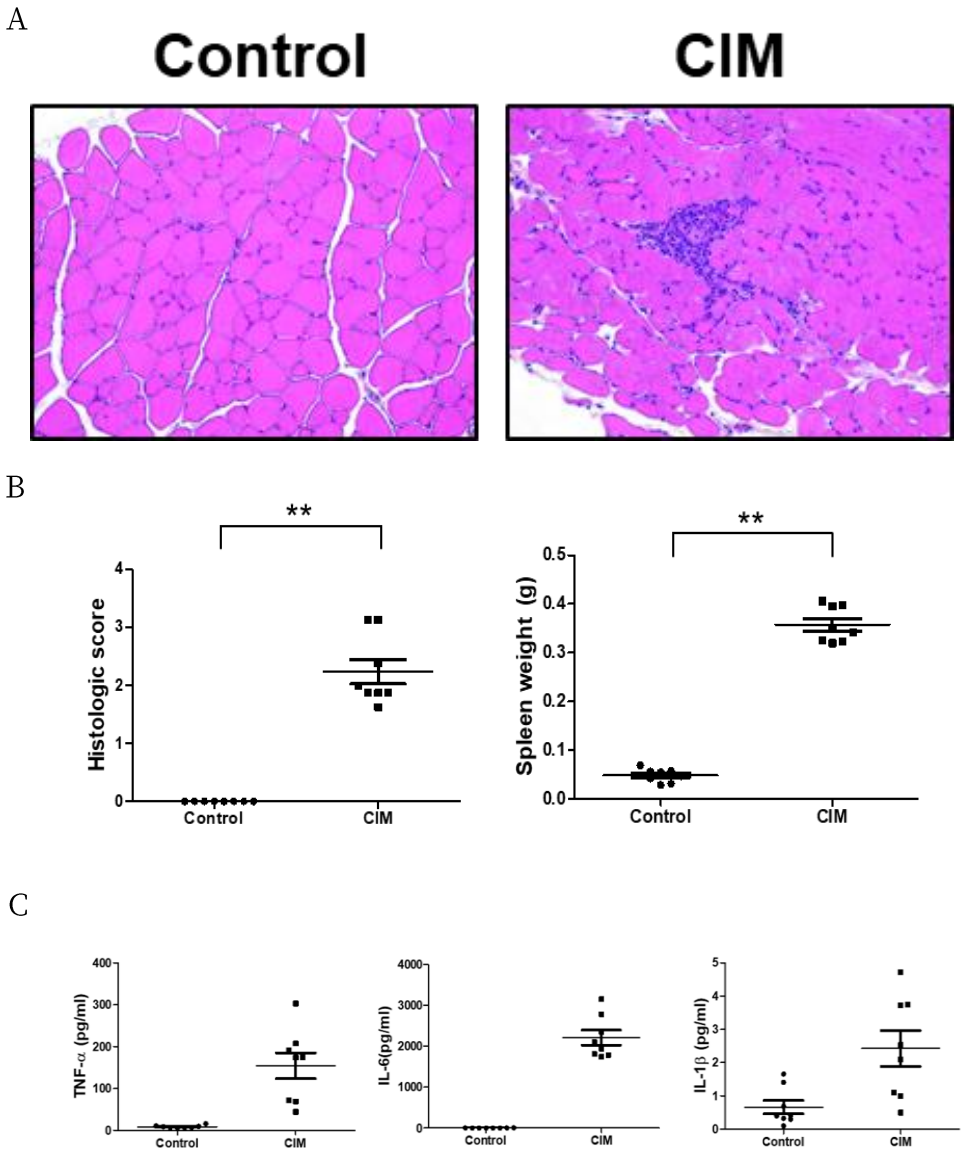

Figure 16. C-protein induced myositis mouse

(A) histology of control and CIM. (B) The histologic score of control and CIM. (** $p < 0.0001$) (C) Increased production of cytokines TNF-α, IL-6, and IL-1 in serum of mouse model.

A

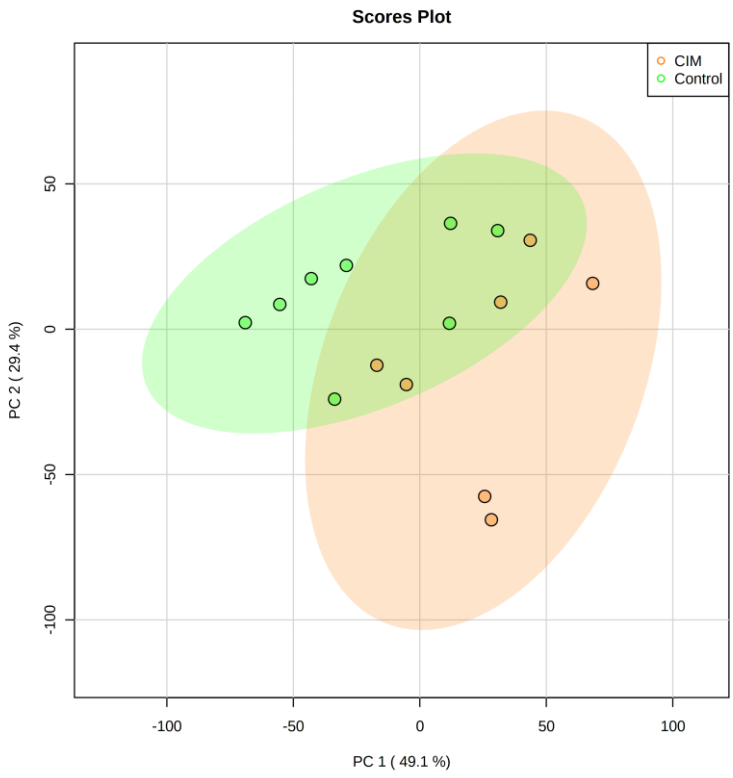
Scores Plot
CIM
Control
PC 2 (29.4 %)
PC 1 (49.1 %)
50
0
-50
-100
-100
-50
0
50
100

B

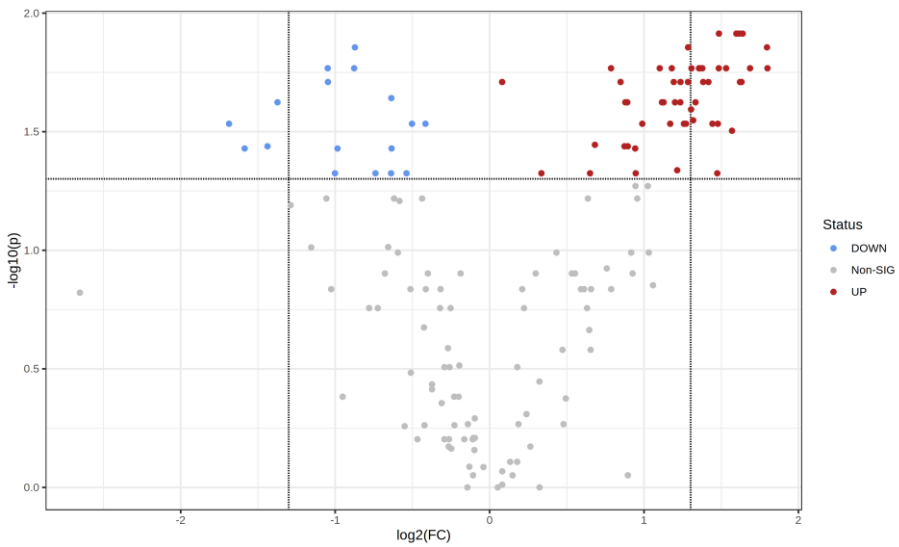
-log10(p)
log2(FC)
Status
DOWN
Non-SIG
UP
2.0
1.5
1.0
0.5
0.0
-2
-1
0
1
2

C

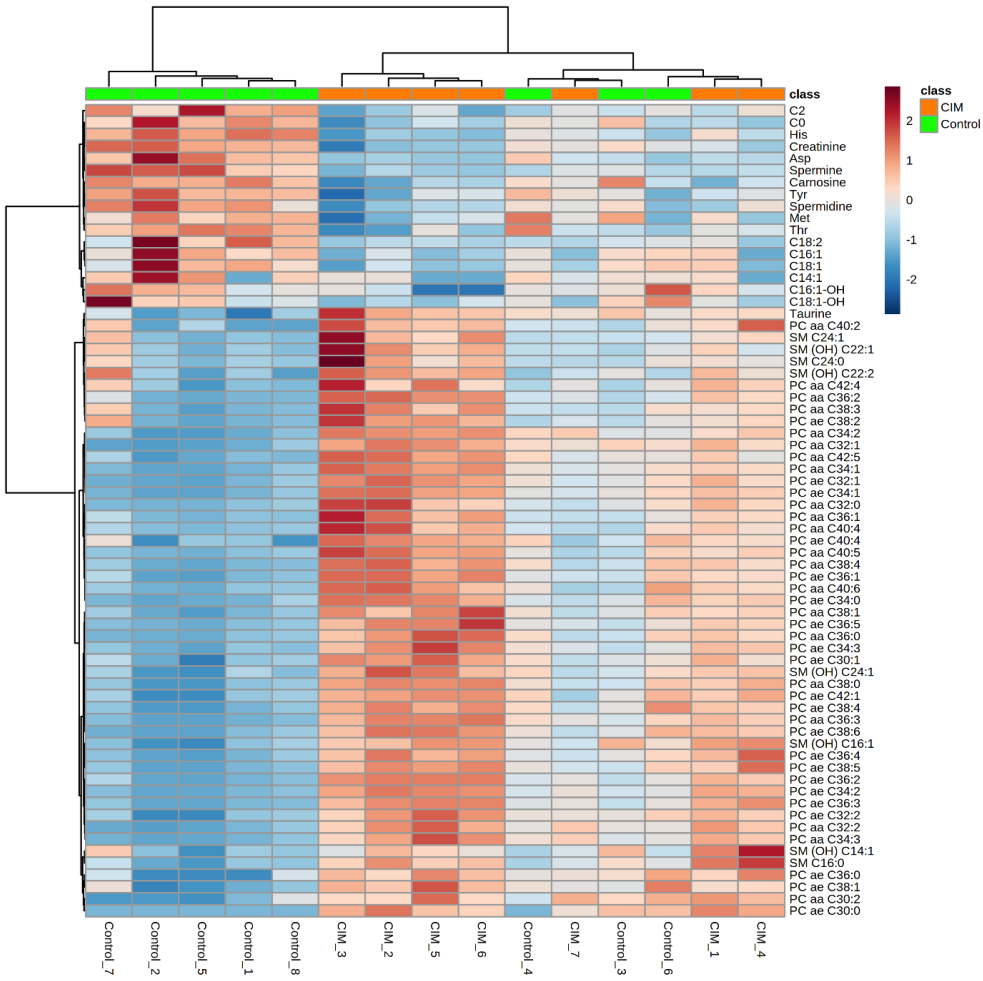

Figure 17. Metabolomic analysis of CIM mouse.

(A) PCA plot of control and CIM skeletal muscle tissue. (B) Volcano plot from t-test results of control and CIM. Red dots are upregulated metabolites, and blue dots are downregulated metabolites. (C) Heatmap of significant metabolites with all mice skeletal muscle samples.

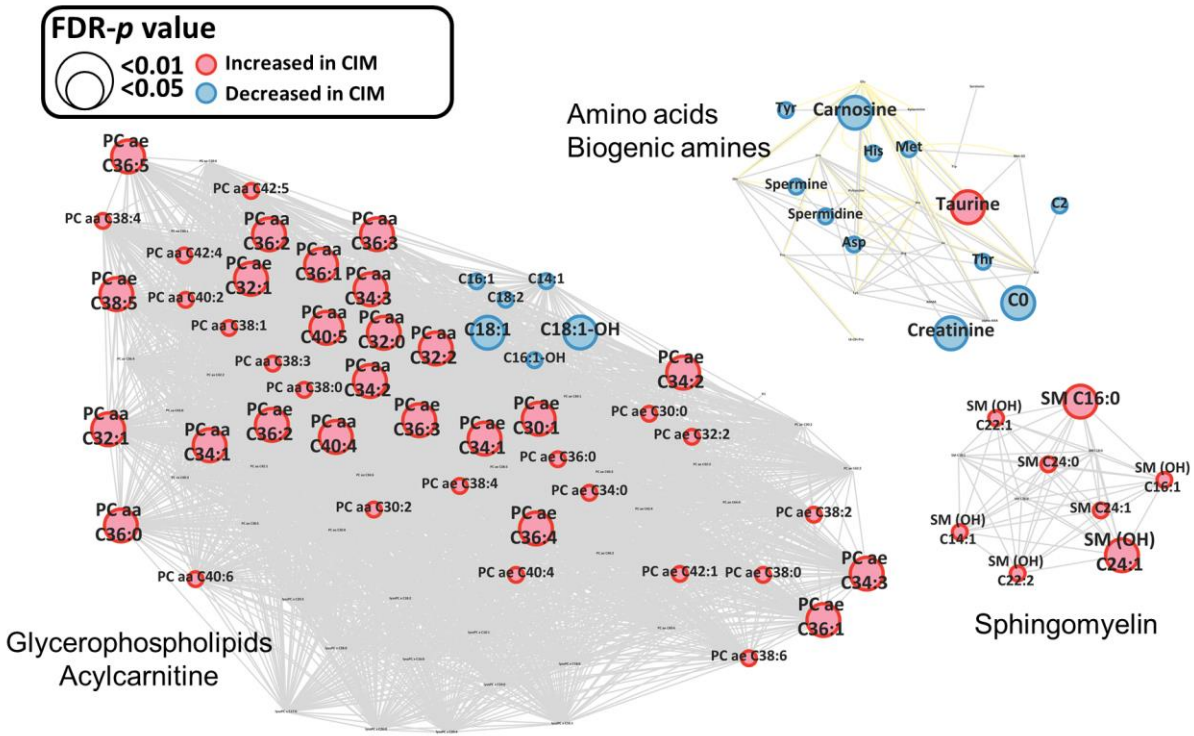

Figure 18. MetaMapp metabolomic networks of mouse tissue, comparing CIM and control.

Border color and node color: red indicates up-regulation in CIM, and blue indicates down-regulation in CIM. Node size indicates the FDR-adjusted p-value.

A

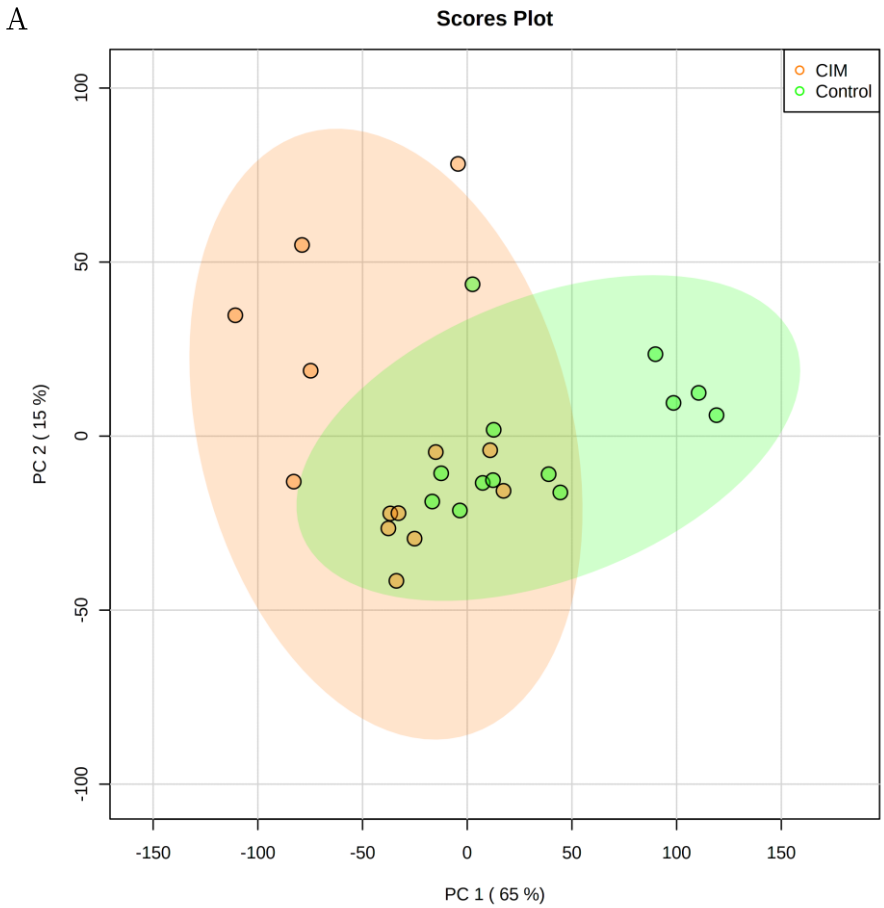
Scores Plot
CIM
Control
PC 2 (15 %)
PC 1 (65 %)
100
50
0
-50
-100
-150
-100
-50
0
50
100
150

B

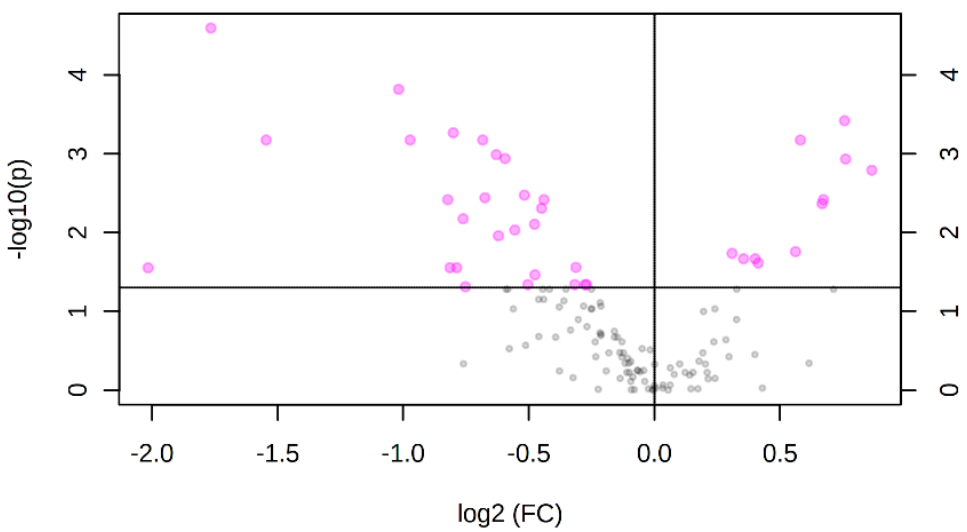
-log10(p)
log2 (FC)
0
1
2
3
4
-2.0
-1.5
-1.0
-0.5
0.0
0.5

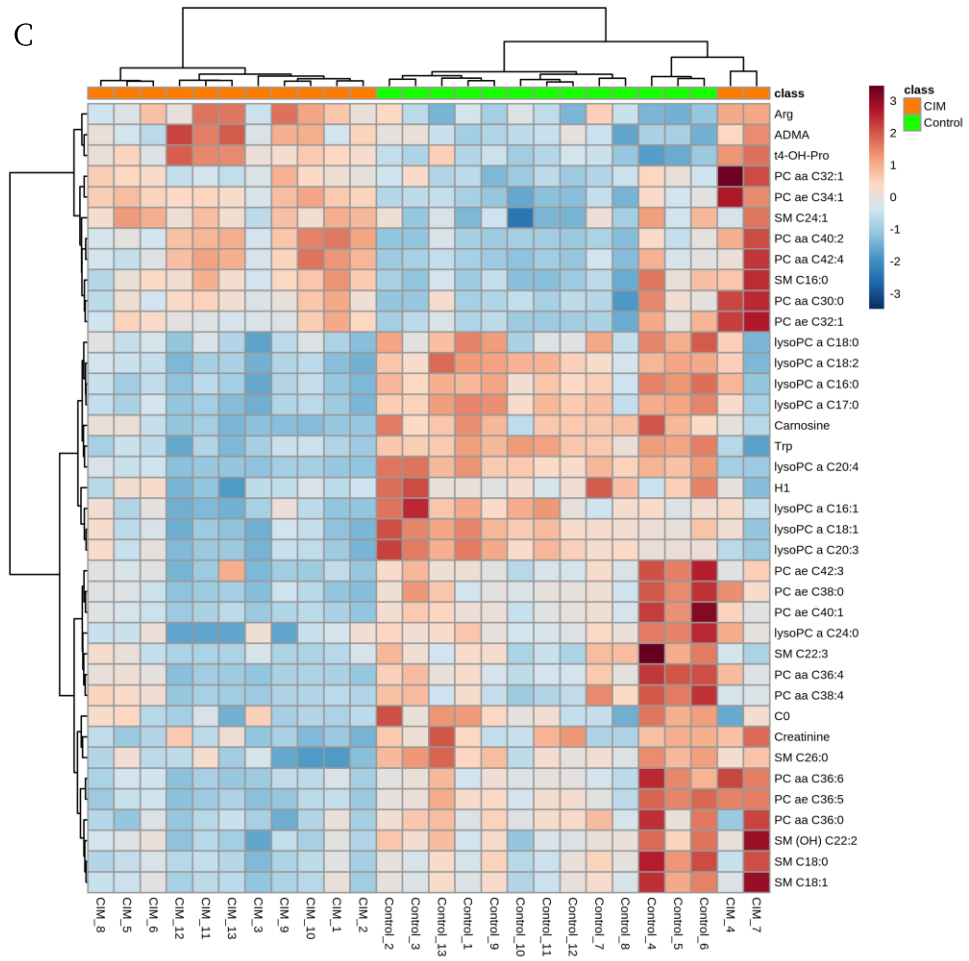

Figure 19. Metabolic profiles in CIM and control mouse serum samples.

(A) PCA plot of control and CIM skeletal muscle serum. (B) Volcano plot from t-test results of control and CIM. (C) Heatmap of significant metabolites with all mice serum samples.

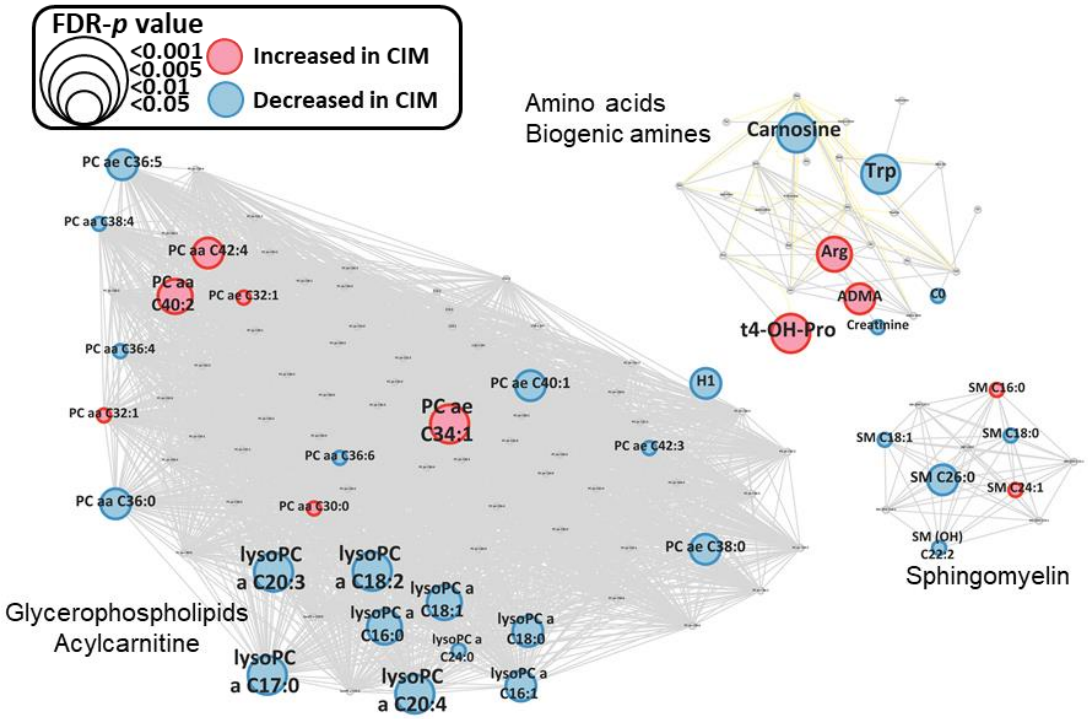

Figure 20. MetaMapp metabolomic networks of mouse serum altered in CIM compared to control.

Border color and node color: red indicates up-regulation in CIM, blue indicates down-regulation in IIM. Node size indicates FDR-adjusted p-value.

8. Metabolic pathway associated with the muscle of CIM mice and expression of ODC-1 and SMOX

After performing statistical analysis on metabolites measured through targeted analysis, an enrichment pathway analysis was performed to identify alterations in metabolic pathways that could potentially be associated with IIM muscle. (Figure 21). The pathway analysis showed that 6 metabolites–aspartic acid, histidine, carnosine, spermidine, and spermine (Figure 22)—were predominantly linked to beta-alanine and histidine metabolism (Table 7). Furthermore, spermine and spermidine were significantly decreased in the CIM mice, indicating the down-regulation of the polyamine pathway (Figure 23). These metabolites have been detected in several studies but were not confirmed in the CIM mouse model (19, 20). Thus, the expression levels of enzymes related to spermine and spermidine were additionally examined. Spermine oxidase (SMOX) converts spermine to spermidine, playing a critical role in the regulation of spermine and spermidine concentration, and ornithine decarboxylase 1 (ODC-1) is known as the rate-limiting enzyme in the polyamine pathway (21, 22). To further understand the alteration of polyamines concentration in muscle tissue, western blot analysis was performed to assess the levels of ODC-1 and SMOX (Figure 24A, B). The expression of ODC-1 increased, whereas SMOX expression decreased in CIM mice.

Table 7. Significantly altered pathway using enrichment analysis in mouse tissue.

Pathway	Total	Hit	Metabolites	P-value
Beta-Alanine metabolism	21	5	L-Aspartic acid, Carnosine, Spermine, L-Histidine, Spermidine	0.0018
Histidine metabolism	16	4	L-Histidine, L-Aspartic acid, Carnosine	0.0315

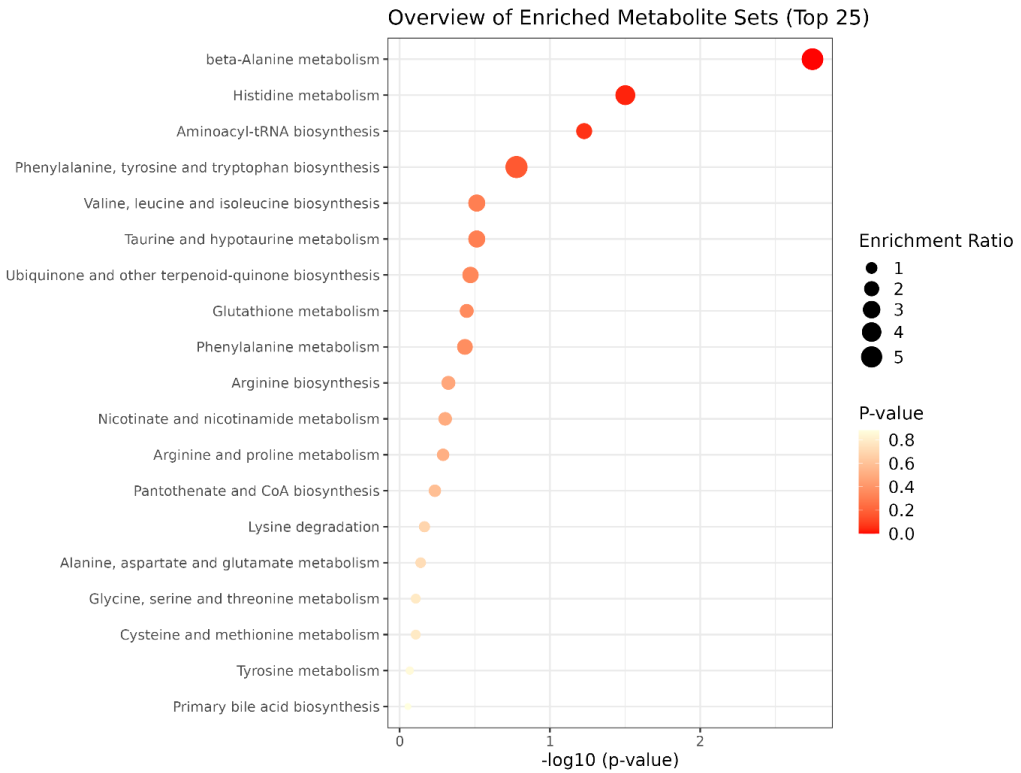

Figure 21. Dot plot of metabolic pathway influenced by statistically significant metabolites.

Color gradient and symbol size represent significant metabolite changes in the corresponding pathway.

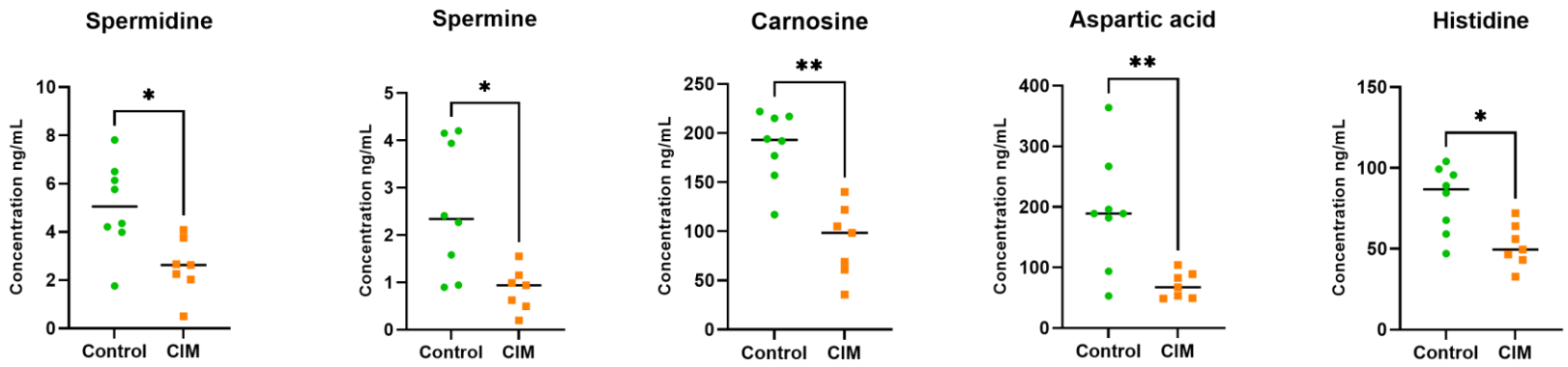

Figure 22. Individual scatter plots of significant metabolites related to important pathways in mouse tissue.

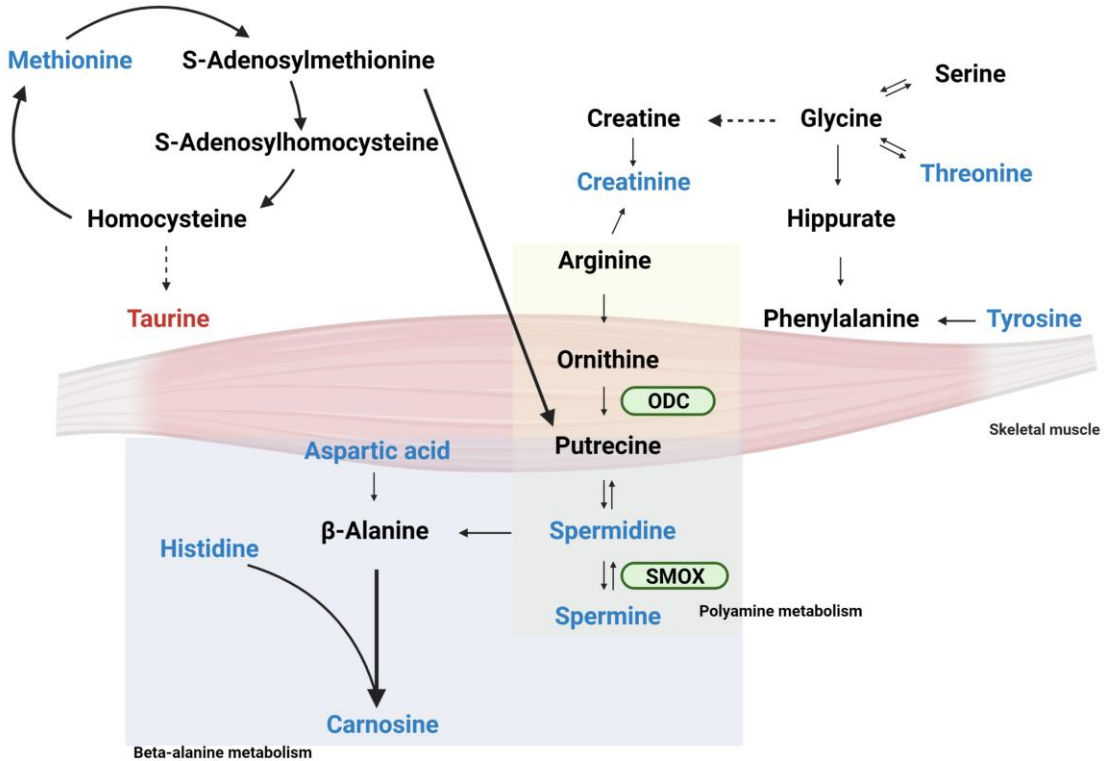

Figure 23. Overview of altered metabolites related to the skeletal muscle tissue of mice.

Red-colored metabolite indicates up-regulation in CIM mice, while blue-colored metabolites represent down-regulation as compared with the control mice.

A

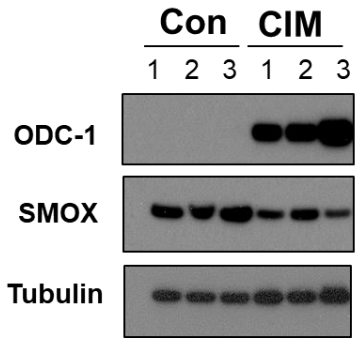

B

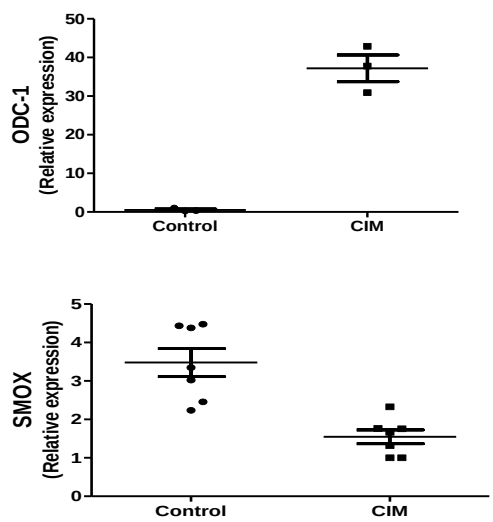

Figure 24. Expression of polyamine metabolic enzymes, ODC-1 and SMOX

(A) Protein expression and (B) relative quantitative data of ODC-1 (** $p < 0.005$), SMOX (** $p < 0.005$), and tubulin.

Discussion

1. IIM-specific metabolites based on targeted metabolomics analysis

Using a targeted metabolomics platform, this study highlights that all groups from patients and healthy control showed different blood metabolic signatures, indicating the potential of the biomarker for IIM and the significant alteration of metabolites to discover the underlying mechanism related to muscle inflammation.

In this study, both targeted metabolomics and untargeted metabolomics analyses were conducted and they revealed distinct trends and patterns among the three groups. In the untargeted metabolomics PCA, a clear separation was observed between the disease-associated inflammation group and the healthy control group. On the other hand, in the targeted metabolomics PCA, the AS group and the healthy control group showed some overlap. It should be noted that targeted metabolomics data represents a limited set of metabolites, whereas untargeted metabolomics data provides an unbiased global metabolic profile that can be associated with inflammation.

Notable metabolites, including five amino acids and two biogenic amines besides lipids, were altered specifically in IIM patients. These

findings are in agreement with those of a previous study that showed serum amino acid concentration alteration in IIM patients (17). Amino acids, especially branched-chain amino acids (BCAA), are essential for skeletal muscle and whole-body metabolism (23). In previous studies, BCAA is recommended as a supplement for muscle development and fatigue treatment (24). However, increased levels of BCAAs can cause inflammation by activating mTORC1, which subsequently increases the production of proinflammatory cytokines (25). The observation of increased BCAA level in the serum in IIM patients needs to be investigated further, along with the levels of other increased amino acids. Remarkably, methionine sulfoxide was specifically increased in IIM patients compared to healthy controls and AS patients, while methionine was decreased in IIM patients compared to healthy control. Methionine sulfoxide, the oxidized form of methionine, can be reduced back to methionine by methionine reductases, which serve as protective mechanisms against oxidative stress and regulate the aging process (26, 27). The altered levels of methionine sulfoxide and methionine are considered biomarkers of oxidative stress, and, therefore, our result might reflect increased ROS production in IIM patients (28, 29).

Additionally, these results showed that various metabolites in the lipid class were altered, specifically in IIM patients. PCs are prominent phospholipids constituting approximately 40–50% of the overall phospholipid content in cell membranes (30). PCs are composed of a

phosphocholine head group connected to two fatty acyl chains via a glycerol backbone. They are predominantly located in the outer layer of the cell membrane, while other glycerophospholipids such as phosphatidylethanolamines, phosphatidylserines, and phosphatidylinositols are primarily found in the inner membrane leaflet. PCs play a crucial role in the initial stages of the inflammatory process (31). Moreover, lysoPCs, the breakdown products of PCs, also contribute to the regulation of the immune system by activating and transporting immune cells. These biological functions have been associated with various inflammatory disorders, including diabetes, obesity, atherosclerosis, cancer, and rheumatoid arthritis (32). Phospholipid metabolism has been highlighted in energy metabolisms, as well as in skeletal muscle function (30). A few studies have reported changes in lipid profiles in the serum of myopathy patients and speculated that dysregulation of the lipid metabolism in patients with polymyositis and dermatomyositis may result in persistent muscle weakness and fatigue (33, 34).

Due to its primary role in facilitating insulin-stimulated glucose disposal, skeletal muscle is widely recognized as the most significant tissue contributing to whole-body insulin resistance (35). In the context of skeletal muscle, insulin resistance is commonly associated with the accumulation of lipids, leading to disruptions in fatty acid (FA) metabolism (36). These disruptions can involve various aspects of FA processing, including altered muscle FA uptake, impaired synthesis of

triacylglycerols (TG), perturbed breakdown of TG (lipolysis), compromised FA oxidation, or a combination of these factors (37). A previous study demonstrated that patients with dermatomyositis were observed with increased insulin resistance (38).

2. Diagnostic biomarker discovery of IIM

In the past few years, machine learning techniques have been widely used to discover biomarkers of muscle diseases. Previous findings have predicted the cancer risk of anti-TIF1γ+ myositis and have suggested gene markers for muscle disease classification using machine learning algorithms. In this study, a set of seven metabolites was identified, which allows for the discrimination of IIM patients from AS patients and healthy controls using machine learning algorithms based on the AUC values of 0.955 (LR), 0.908 (RF) and 0.918 (SVM) (39, 40). These results highlight the potential of using this set of metabolites as a predictive biomarker for IIM patients, providing insights into the underlying pathophysiologic mechanisms of IIM. This biomarker discovery may help in the diagnosis or disease activity monitoring, replacing the need for invasive procedures such as muscle biopsies.

3. Muscle inflammation induces alteration of oxylipins

Upon cleavage of PCs containing a fatty acyl group known as C20:4, arachidonic acid (20:4) is released, which serves as the precursor for a group of oxylipins and eicosanoids (32). In this study, a significant decrease in lysoPC a C20:4 was observed in patients with IIM compared to healthy controls. However, no significant change was observed in arachidonic acid levels. Interestingly, three oxylipins derived from arachidonic acid, 9-HETE, 11-HETE, and 8-HEPE, showed a significant increase in IIM patients compared to the healthy control group. Oxylipins are lipid mediators synthesized from polyunsaturated fatty acids (PUFAs), which are categorized into two groups: omega-6 (n-6) and omega-3 (n-3), based on the position of the final double bond from the end of the carbon chain. Similarly, oxylipins are also categorized into n-6 and n-3 subtypes as PUFA metabolites (41, 42). Omega-3 PUFAs, such as eicosapentaenoic acid (EPA; C20:5n-3) and docosahexaenoic acid (DHA; C22:6n-3), are known to produce functional anti-inflammatory mediators, including protectins and resolvins, which are effective in both acute and chronic inflammatory conditions (43). On the other hand, arachidonic acid (AA), a representative omega-6 PUFA, is extensively studied due to its association with the inflammatory response (44). In this study, oxylipin levels were significantly increased in IIM patients compared

to healthy controls, whereas previous studies showed opposite results and demonstrated the effect of myositis on muscle performance (17). However, individual oxylipin levels were observed in this study, and further studies are needed to clarify the role of oxylipins related to inflammation in muscle.

4. Pathophysiology of IIM in mouse muscle tissue

In the muscle tissue of CIM mice, spermine and spermidine from the polyamine pathway were significantly down-regulated in this study. In addition, ornithine and putrescine, which also are involved in the polyamine pathway, were significantly increased in the serum of IIM patients compared to healthy controls. Previous studies have described dysregulated polyamine metabolism associated with various diseases and inflammation (45, 46). Polyamines in muscle diseases are related to the degeneration and regeneration of muscular fibers, and the concentrations of spermine and spermidine are regulated by a key enzyme, SMOX (47). Furthermore, SMOX expression was also reduced, along with the decreased spermine and spermidine concentrations, in CIM mice. A recent study demonstrated that a significant reduction of SMOX expression is associated with muscle atrophy induced by various conditions (48). Aging is one of the conditions that can reduce spermidine levels and SMOX expression, which can bring about a loss of skeletal muscle (49). The significant reduction of spermine, spermidine, and SMOX expression and significant induction of ODC was highly consistent with that in aged skeletal muscle. These alterations in metabolites and enzyme expression may be affected by aging, which involves decreased cell proliferation and protein synthesis (50). Thus, the

alterations in polyamine metabolites and associated enzymes might reflect an aging phenotype in inflammatory muscle.

Moreover, enrichment pathway analysis revealed changes in metabolites related to beta-alanine and histidine metabolisms. Compared to the control mice, histidine, carnosine, and aspartic acid levels were lower in the muscle tissue of CIM mice. Carnosine, formed from histidine and beta-alanine, is highly present and primarily synthesized in skeletal muscle tissue in mammals (51). In addition, carnosine has protective effects, including the reduction of proinflammatory and profibrotic cytokines, which can suppress ROS production and inflammation (52, 53). Histidine also plays an important role in skeletal muscle by enhancing muscle performance and contributing to the synthesis of carnosine (54). The decrease in muscle carnosine and histidine levels may reflect cell damage in the presence of inflammation.

In our study, interestingly, metabolic profiling in tissue samples from CIM mice showed that metabolites from each class, except taurine, changed in the same direction. The significant reduction in several amino acids and amines, such as aspartic acid, histidine, methionine, threonine, tyrosine, carnosine, creatinine, spermidine, and spermine, observed in our study is highly consistent with previous studies on aging. Essential amino acids stimulate protein synthesis in skeletal muscle, and the delivery of amino acids is closely associated with muscle weakness and atrophy (55). Previous studies further

showed that reduced amino acid delivery and protein synthesis are stimulated by mTORC1 in aged skeletal muscle (56). Our findings in this study have particular relevance to the aging phenotype. Additionally, significant metabolites in human serum were compared with those in mouse tissue to investigate the association between these samples. It was observed that the majority of significant metabolites identified in mouse tissue did not exhibit significant changes in human serum in this study. While the mouse model is commonly utilized as a disease model, it is important to consider the potential impact of species differences on metabolic processes in pathophysiology. Moreover, the present study included various subtypes of IIM in human patients, whereas the mouse model only mimicked polymyositis, significantly influencing our findings.

5. Study limitations

The limitations of the present study include the lack of a validation cohort for modeling, the small sample size of patient groups and healthy controls, the lack of various disease controls, and the potential gender difference of polyamine metabolites in the mouse model. The lack of a validation set in this study poses a risk of model overfitting. As IIM is a rare disease, it was challenging to recruit an additional validation cohort. To overcome this limitation, the five-fold cross-validation method with three machine learning algorithms was practiced. Additionally, one of the limitations is the small sample size. Therefore, IIM specific metabolites and the diagnostic metabolite panel remain to be further investigated using larger cohorts to validate these results.

Conclusion

In summary, this study utilized targeted and untargeted metabolomics profiling to identify a specific metabolic signature in both serum and inflamed tissue of IIM patients. To the best of our knowledge, this is the first study to propose a metabolic biomarker for IIM patients using a machine learning algorithm-based prediction model. Beyond suggesting a predictive marker of IIM, our study additionally uncovered alteration of metabolites related to muscle inflammation and provided new insights into IIM pathology.

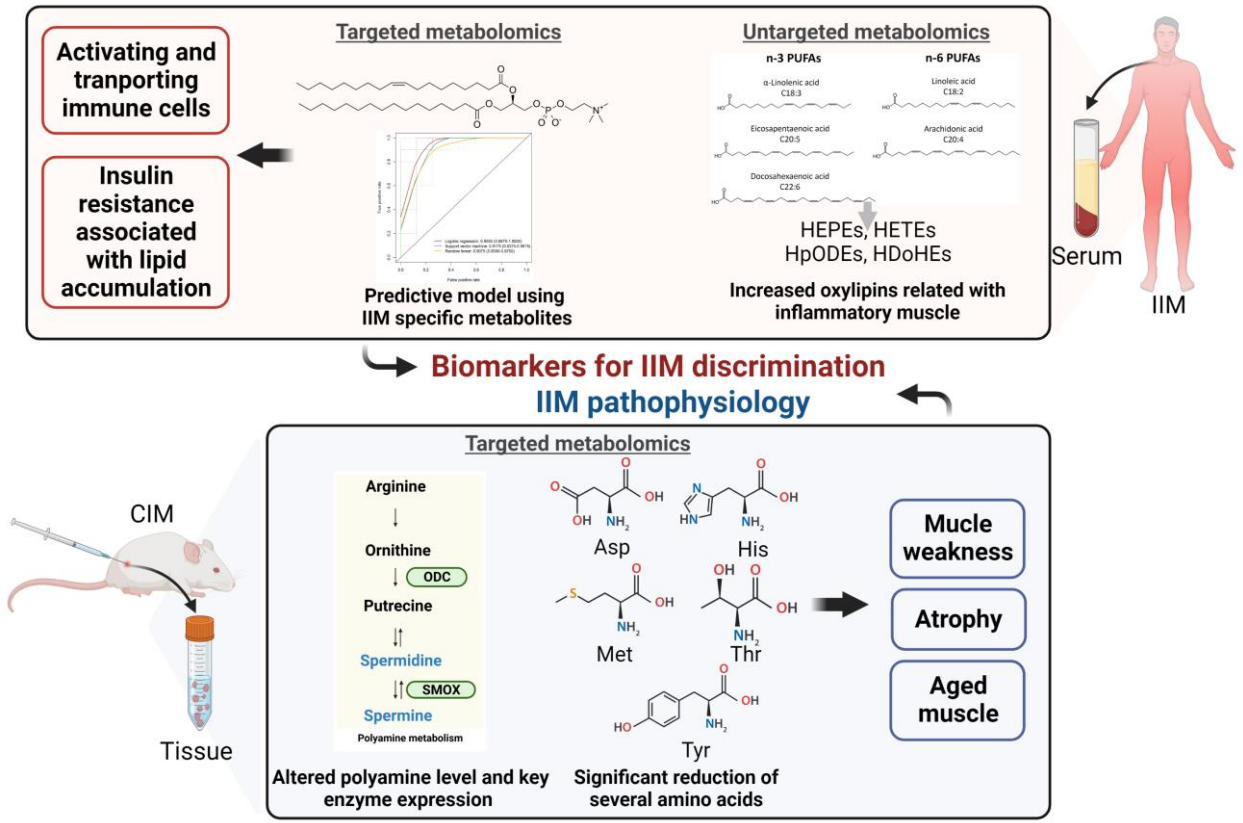

Figure 25. Summary of the dissertation

References

1. Dalakas MC. Inflammatory Muscle Diseases. N Engl J Med. 2015;373(4):393-4.
2. Rayavarapu S, Coley W, Kinder TB, Nagaraju K. Idiopathic inflammatory myopathies: pathogenic mechanisms of muscle weakness. Skelet Muscle. 2013;3(1):13.
3. Rothwell S, Cooper RG, Lamb JA, Chinoy H. Strategies for evaluating idiopathic inflammatory myopathy disease susceptibility genes. Curr Rheumatol Rep. 2014;16(10):446.
4. Meyer A, Meyer N, Schaeffer M, Gottenberg JE, Geny B, Sibilia J. Incidence and prevalence of inflammatory myopathies: a systematic review. Rheumatology (Oxford). 2015;54(1):50-63.
5. Bohan A, Peter JB. Polymyositis and dermatomyositis (first of two parts). N Engl J Med. 1975;292(7):344-7.
6. Bohan A, Peter JB. Polymyositis and dermatomyositis (second of two parts). N Engl J Med. 1975;292(8):403-7.
7. McHugh NJ, Tansley SL. Autoantibodies in myositis. Nat Rev Rheumatol. 2018;14(5):290-302.
8. Betteridge Z, Tansley S, Shaddick G, Chinoy H, Cooper R, New R, et al. Frequency, mutual exclusivity and clinical associations of myositis autoantibodies in a combined European cohort of idiopathic inflammatory myopathy patients. Journal of autoimmunity. 2019;101:48-55.
9. Sugihara T, Sekine C, Nakae T, Kohyama K, Harigai M, Iwakura Y, et al. A new murine model to define the critical pathologic and therapeutic mediators of polymyositis. Arthritis Rheum. 2007;56(4):1304-14.

10. Okiyama N, Sugihara T, Iwakura Y, Yokozeki H, Miyasaka N, Kohsaka H. Therapeutic effects of interleukin-6 blockade in a murine model of polymyositis that does not require interleukin-17A. Arthritis Rheum. 2009;60(8):2505-12.
11. Sugihara T, Okiyama N, Suzuki M, Kohyama K, Matsumoto Y, Miyasaka N, et al. Definitive engagement of cytotoxic CD8 T cells in C protein-induced myositis, a murine model of polymyositis. Arthritis Rheum. 2010;62(10):3088-92.
12. Braun J, Sieper J. Ankylosing spondylitis. Lancet. 2007;369(9570):1379-90.
13. Waragai M, Shinotoh H. Ankylosing spondylitis associated with myositis. J Neurol Neurosurg Psychiatry. 1994;57(5):661-2.
14. Liu D, Zuo X, Luo H, Zhu H. The altered metabolism profile in pathogenesis of idiopathic inflammatory myopathies. Semin Arthritis Rheum. 2020;50(4):627-35.
15. Johnson CH, Ivanisevic J, Siuzdak G. Metabolomics: beyond biomarkers and towards mechanisms. Nat Rev Mol Cell Biol. 2016;17(7):451-9.
16. Saoi M, Britz-McKibbin P. New Advances in Tissue Metabolomics: A Review. Metabolites. 2021;11(10).
17. Guleria A, Kumar U, Kumar D, R N, Anuja AK, Singh MK, et al. NMR - based serum and muscle metabolomics for diagnosis and activity assessment in idiopathic inflammatory myopathies. Analytical Science Advances. 2021;2(11-12):515-26.
18. Pang Z, Chong J, Zhou G, de Lima Morais DA, Chang L, Barrette M, et al. MetaboAnalyst 5.0: narrowing the gap between raw spectra and functional insights. Nucleic Acids Res. 2021;49(W1):W388-W96.
19. Tabbaa M, Ruz Gomez T, Campelj DG, Gregorevic P, Hayes A, Goodman CA. The regulation of polyamine pathway proteins in

models of skeletal muscle hypertrophy and atrophy: a potential role for mTORC1. Am J Physiol Cell Physiol. 2021;320(6):C987-C99.
20. Kaminska AM, Stern LZ, Russell DH. Polyamine metabolism in muscle: differential response to tenotomy and denervation in the soleus and gastrocnemius muscle of adult rats. Exp Neurol. 1982;78(2):331-9.
21. Wu DH, Kaan HYK, Zheng XX, Tang XH, He Y, Tan QV, et al. Structural basis of Ornithine Decarboxylase inactivation and accelerated degradation by polyamine sensor Antizyme1. Sci Rep-Uk. 2015;5.
22. Gobert AP, Al-Greene NT, Singh K, Coburn LA, Sierra JC, Verriere TG, et al. Distinct Immunomodulatory Effects of Spermine Oxidase in Colitis Induced by Epithelial Injury or Infection. Front Immunol. 2018;9:1242.
23. Mann G, Mora S, Madu G, Adegoke OAJ. Branched-chain Amino Acids: Catabolism in Skeletal Muscle and Implications for Muscle and Whole-body Metabolism. Front Physiol. 2021;12:702826.
24. Holecek M. The role of skeletal muscle in the pathogenesis of altered concentrations of branched-chain amino acids (valine, leucine, and isoleucine) in liver cirrhosis, diabetes, and other diseases. Physiol Res. 2021;70(3):293-305.
25. Ye Z, Wang S, Zhang C, Zhao Y. Coordinated Modulation of Energy Metabolism and Inflammation by Branched-Chain Amino Acids and Fatty Acids. Front Endocrinol (Lausanne). 2020;11:617.
26. Cabreiro F, Picot CR, Friguet B, Petropoulos I. Methionine sulfoxide reductases: relevance to aging and protection against oxidative stress. Ann N Y Acad Sci. 2006;1067:37-44.
27. Moskovitz J. Methionine sulfoxide reductases: ubiquitous enzymes involved in antioxidant defense, protein regulation, and

prevention of aging-associated diseases. Biochim Biophys Acta. 2005;1703(2):213-9.
28. Suzuki S, Kodera Y, Saito T, Fujimoto K, Momozono A, Hayashi A, et al. Methionine sulfoxides in serum proteins as potential clinical biomarkers of oxidative stress. Sci Rep. 2016;6:38299.
29. Muller FL, Lustgarten MS, Jang Y, Richardson A, Van Remmen H. Trends in oxidative aging theories. Free Radic Biol Med. 2007;43(4):477-503.
30. van der Veen JN, Kennelly JP, Wan S, Vance JE, Vance DE, Jacobs RL. The critical role of phosphatidylcholine and phosphatidylethanolamine metabolism in health and disease. Biochim Biophys Acta Biomembr. 2017;1859(9 Pt B):1558-72.
31. Cas MD, Roda G, Li F, Secundo F. Functional Lipids in Autoimmune Inflammatory Diseases. Int J Mol Sci. 2020;21(9).
32. Yamashita A, Hayashi Y, Nemoto-Sasaki Y, Ito M, Oka S, Tanikawa T, et al. Acyltransferases and transacylases that determine the fatty acid composition of glycerolipids and the metabolism of bioactive lipid mediators in mammalian cells and model organisms. Prog Lipid Res. 2014;53:18-81.
33. Raouf J, Idborg H, Englund P, Alexanderson H, Dastmalchi M, Jakobsson PJ, et al. Targeted lipidomics analysis identified altered serum lipid profiles in patients with polymyositis and dermatomyositis. Arthritis Res Ther. 2018;20(1):83.
34. Dabaj I, Ferey J, Marguet F, Gilard V, Basset C, Bahri Y, et al. Muscle metabolic remodelling patterns in Duchenne muscular dystrophy revealed by ultra-high-resolution mass spectrometry imaging. Sci Rep. 2021;11(1):1906.
35. Borkman M, Storlien LH, Pan DA, Jenkins AB, Chisholm DJ, Campbell LV. The relation between insulin sensitivity and the

fatty-acid composition of skeletal-muscle phospholipids. N Engl J Med. 1993;328(4):238-44.

36. Storlien LH, Jenkins AB, Chisholm DJ, Pascoe WS, Khouri S, Kraegen EW. Influence of dietary fat composition on development of insulin resistance in rats. Relationship to muscle triglyceride and omega-3 fatty acids in muscle phospholipid. Diabetes. 1991;40(2):280-9.
37. Itani SI, Ruderman NB, Schmieder F, Boden G. Lipid-induced insulin resistance in human muscle is associated with changes in diacylglycerol, protein kinase C, and IkappaB-alpha. Diabetes. 2002;51(7):2005-11.
38. Oliveira DSd, Guimarães MS, Shinjo SK. Insulin resistance is increased in adult patients with dermatomyositis. Medical Express. 2018;5(0).
39. Tran A, Walsh CJ, Batt J, Dos Santos CC, Hu P. A machine learning-based clinical tool for diagnosing myopathy using multi-cohort microarray expression profiles. J Transl Med. 2020;18(1):454.
40. Zhao L, Xie S, Zhou B, Shen C, Li L, Pi W, et al. Machine Learning Algorithms Identify Clinical Subtypes and Cancer in Anti-TIF1gamma+ Myositis: A Longitudinal Study of 87 Patients. Front Immunol. 2022;13:802499.
41. Rizos EC, Ntzani EE, Bika E, Kostapanos MS, Elisaf MS. Association Between Omega-3 Fatty Acid Supplementation and Risk of Major Cardiovascular Disease Events A Systematic Review and Meta-analysis. Jama-J Am Med Assoc. 2012;308(10):1024-33.
42. Weinberg RL, Brook RD, Rubenfire M, Eagle KA. Cardiovascular Impact of Nutritional Supplementation With Omega-3 Fatty Acids JACC Focus Seminar. J Am Coll Cardiol. 2021;77(5):593-608.

43. Misheva M, Johnson J, McCullagh J. Role of Oxylipins in the Inflammatory-Related Diseases NAFLD, Obesity, and Type 2 Diabetes. Metabolites. 2022;12(12).
44. Samuelsson B. Arachidonic-Acid Metabolism - Role in Inflammation. Z Rheumatol. 1991;50:3-6.
45. Mahajan UV, Varma VR, Griswold ME, Blackshear CT, An Y, Oommen AM, et al. Dysregulation of multiple metabolic networks related to brain transmethylation and polyamine pathways in Alzheimer disease: A targeted metabolomic and transcriptomic study. PLoS Med. 2020;17(1):e1003012.
46. Park MH, Igarashi K. Polyamines and Their Metabolites as Diagnostic Markers of Human Diseases. Biomol Ther. 2013;21(1):1-9.
47. Cervelli M, Leonetti A, Duranti G, Sabatini S, Ceci R, Mariottini P. Skeletal Muscle Pathophysiology: The Emerging Role of Spermine Oxidase and Spermidine. Med Sci (Basel). 2018;6(1).
48. Bongers KS, Fox DK, Kunkel SD, Stebounova LV, Murry DJ, Pufall MA, et al. Spermine oxidase maintains basal skeletal muscle gene expression and fiber size and is strongly repressed by conditions that cause skeletal muscle atrophy. Am J Physiol Endocrinol Metab. 2015;308(2):E144-58.
49. Eisenberg T, Knauer H, Schauer A, Buttner S, Ruckenstuhl C, Carmona-Gutierrez D, et al. Induction of autophagy by spermidine promotes longevity. Nat Cell Biol. 2009;11(11):1305-14.
50. Uchitomi R, Hatazawa Y, Senoo N, Yoshioka K, Fujita M, Shimizu T, et al. Metabolomic Analysis of Skeletal Muscle in Aged Mice. Sci Rep. 2019;9(1):10425.
51. Boldyrev AA, Aldini G, Derave W. Physiology and pathophysiology of carnosine. Physiol Rev. 2013;93(4):1803-45.

52. Cuzzocrea S, Genovese T, Failla M, Vecchio G, Fruciano M, Mazzon E, et al. Protective effect of orally administered carnosine on bleomycin-induced lung injury. Am J Physiol Lung Cell Mol Physiol. 2007;292(5):L1095-104.
53. Kubota M, Kobayashi N, Sugizaki T, Shimoda M, Kawahara M, Tanaka KI. Carnosine suppresses neuronal cell death and inflammation induced by 6-hydroxydopamine in an in vitro model of Parkinson's disease. PLoS One. 2020;15(10):e0240448.
54. Holecek M, Vodenicarovova V. Effects of histidine supplementation on amino acid metabolism in rats. Physiol Res. 2020;69(1):99-111.
55. Volpi E, Sheffield-Moore M, Rasmussen BB, Wolfe RR. Basal muscle amino acid kinetics and protein synthesis in healthy young and older men. JAMA. 2001;286(10):1206-12.
56. Moro T, Ebert SM, Adams CM, Rasmussen BB. Amino Acid Sensing in Skeletal Muscle. Trends Endocrinol Metab. 2016;27(11):796-806.

국문 초록

서 론: 특발성 염증성 근육 병증은 자가면역 질환으로, 여러가지 임상 증상, 치료에 대한 반응, 예후가 다양하게 나타난다. 또한, 근생검 없이는 정확한 진단이 어렵다. 본 연구에서는 특발성 염증성 근육 병증 환자를 진단할 수 있는 대사체 패널을 식별하고 환자의 혈청과 마우스 모델의 근육에서 특발성 염증성 근육 병증 특이적인 대사체 특징을 탐색하고자 하였다.

방 법: 특발성 염증성 근육 병증 환자 50 명, 강직성 척추염 환자 30 명, 건강인 10 명의 혈청과, 마우스 모델의 근육조직 및 혈청을 수집하였다. 모든 시료는 액체크로마토프/질량분석기 기반 표적대사체 분석으로 진행되었고 일부 환자시료와 건강인 시료로 비표적 대사체 분석도 진행하였다. 단변량, 다변량 분석을 통하여 대사체들의 변화를 확인하고 3 가지 머신러닝 방법인 로지스틱 회기분석 (LR), support vector machine (SVM), 및 random forest (RF)를 이용하여 특발성 염증성 근육병증을 예측할 수 있는 모델을 구축하였다.

결 과: 37 개의 IIM 특이적인 대사체 중 후진 소거법을 이용하여 7 개의 예측 바이오마커를 발굴하였다. 구축된 모델은 5-fold 교차 검증을 통해 3 가지 머신러닝 방법으로 평가되었다. 각 분류 모델에 대해 ROC curve 의 AUC 값은 0.955 (LR), 0.908 (RF) and 0.918 (SVM)로 산출되었다. 추가적으로 특발성 염증성 근육 병증 환자 군에서 옥시리핀이 유의하게 증가한 것을 확인하였다. 마우스 모델 조직 시료에서는, CIM 군에서 총 68 개의 대사체가 유의하게 변화하였다. 타우린을 제외한 모든 대사체들은

클래스별로 CIM 쥐에서 동일한 양상으로 변화하였다. 특히, 경로 분석을 통해 근육 염증에 기여하는 가장 영향력 있는 경로는 polyamine 대사 경로와 beta-alanine 대사 경로인 것을 확인하였다.

결 론: 다양한 시료와 대사체방법론을 이용하여 특발성 염증성 근육 병증의 질병 기전이 노화 및 염증 관련 특징이 있는 것을 확인하였고 추가적으로 진단 가능성있는 대사체 바이오마커 패널을 제시하였다.

* 본 내용의 일부는 Metabolites 학술지 (Kang J and Kim J, et al. Identification of Metabolic Signature Associated with Idiopathic Inflammatory Myopathy Reveals Polyamine Pathway Alteration in Muscle Tissue. Metabolites. 2022;12(10)에 한편의 원저로 출판 완료된 내용임.

주요어: 특발성 염증성 근육 병증, 대사체학, C protein-induced myositis 마우스모델, 바이오마커, 질병기전

학 번: 2017-25272